

# Total Absorption $\gamma$ -Ray Spectroscopy of $^{87}\text{Br}$ , $^{88}\text{Br}$ and $^{94}\text{Rb}$ $\beta$ -Delayed Neutron Emitters

E. Valencia, J. L. Tain,\* A. Algora,† J. Agramunt, E. Estevez, M.D. Jordan, and B. Rubio  
*Instituto de Fisica Corpuscular (CSIC-Universitat de Valencia), Apdo. Correos 22085, E-46071 Valencia, Spain*

S. Rice, P. Regan, W. Gelletly, Z. Podolyák, M. Bowry, P. Mason, and G. F. Farrelly  
*University of Surrey, Department of Physics, Guildford GU2 7XH, United Kingdom*

A. Zakari-Issoufou, M. Fallot, A. Porta, and V. M. Bui  
*SUBATECH, CNRS/IN2P3, Universit de Nantes, Ecole des Mines, F-44307 Nantes, France*

J. Rissanen, T. Eronen, I. Moore, H. Penttilä, J. Äystö, V.-V. Elomaa, J. Hakala, A. Jokinen, V. S. Kolhinen, M. Reponen, and V. Sonnenschein  
*University of Jyväskylä, Department of Physics, P.O. Box 35, FI-40014 University of Jyväskylä, Finland*

D. Cano-Ott, A. R. Garcia, T. Martínez, and E. Mendoza  
*Centro de Investigaciones Energéticas Medioambientales y Tecnológicas, E-28040 Madrid, Spain*

R. Caballero-Folch, B. Gomez-Hornillos, and V. Gorlichev  
*Universitat Politècnica de Catalunya, E-08028 Barcelona, Spain*

F. G. Kondev  
*Nuclear Engineering Division, Argonne National Laboratory, Argonne, Illinois 60439, USA*

A. A. Sonzogni  
*NNDC, Brookhaven National Laboratory, Upton, New York 11973, USA*

L. Batist  
*Petersburg Nuclear Physics Institute, Gatchina, Russia*  
 (Dated: September 21, 2016)

We investigate the decay of  $^{87,88}\text{Br}$  and  $^{94}\text{Rb}$  using total absorption  $\gamma$ -ray spectroscopy. These important fission products are  $\beta$ -delayed neutron emitters. Our data show considerable  $\beta\gamma$ -intensity, so far unobserved in high-resolution  $\gamma$ -ray spectroscopy, from states at high excitation energy. We also find significant differences with the  $\beta$  intensity that can be deduced from existing measurements of the  $\beta$  spectrum. We evaluate the impact of the present data on reactor decay heat using summation calculations. Although the effect is relatively small it helps to reduce the discrepancy between calculations and integral measurements of the photon component for  $^{235}\text{U}$  fission at cooling times in the range 1 – 100 s. We also use summation calculations to evaluate the impact of present data on reactor antineutrino spectra. We find a significant effect at antineutrino energies in the range of 5 to 9 MeV. In addition, we observe an unexpected strong probability for  $\gamma$  emission from neutron unbound states populated in the daughter nucleus. The  $\gamma$  branching is compared to Hauser-Feshbach calculations which allow one to explain the large value for bromine isotopes as due to nuclear structure. However the branching for  $^{94}\text{Rb}$ , although much smaller, hints of the need to increase the radiative width  $\Gamma_\gamma$  by one order-of-magnitude. This leads to a similar increase in the calculated  $(n, \gamma)$  cross section for this very neutron-rich nucleus with a potential impact on  $r$  process abundance calculations.

## I. INTRODUCTION

Neutron-unbound states can be populated in the  $\beta$ -decay of very neutron-rich nuclei, when the neutron separation energy  $S_n$  in the daughter nucleus is lower than

the decay energy window  $Q_\beta$ . The relative strength of strong and electromagnetic interactions determines the preponderance of neutron emission over  $\gamma$ -ray emission from these states. These emission rates are quantified by the partial level widths  $\Gamma_n$  and  $\Gamma_\gamma$  respectively. The fraction of  $\beta$  intensity followed by  $\gamma$ -ray emission is given by  $\Gamma_\gamma/\Gamma_{tot}$ , with  $\Gamma_{tot} = \Gamma_\gamma + \Gamma_n$ . There is an analogy [1] between this decay process and neutron capture reactions populating unbound states. Such resonances in the compound nucleus re-emit a neutron (elastic channel) or

\* Corresponding author: tain@ific.uv.es

† Institute of Nuclear Research of the Hungarian Academy of Sciences, H-4026 Debrecen, Hungary

de-excite by  $\gamma$ -rays (radiative capture). Indeed the reaction cross section is parametrized in terms of neutron and  $\gamma$  widths. In particular the  $(n, \gamma)$  cross section includes terms proportional to  $\Gamma_\gamma \Gamma_n / \Gamma_{tot}$ . Notice that the spins and parities of states populated in  $\beta$ -decay and  $(n, \gamma)$  do not coincide in general because of the different selection rules.

Neutron capture and transmission reactions have been extensively used [2] to determine  $\Gamma_\gamma$  and  $\Gamma_n$  of resolved resonances, or the related strength functions in the unresolved resonance region. An inspection of Ref. [2] shows that in general  $\Gamma_n$  is measured in eV or keV while  $\Gamma_\gamma$  is measured in meV or eV, in agreement with expectation. Current data is restricted, however, to nuclei close to stability since such experiments require the use of stable or long-lived targets. On the other hand,  $(n, \gamma)$  capture cross sections for very neutron-rich nuclei are a key ingredient in reaction network calculations describing the synthesis of elements heavier than iron during the rapid ( $r$ ) neutron capture process occurring in explosive-like stellar events. In the classical picture of the  $r$  process [3] a large burst of neutrons synthesizes the elements along a path determined by the  $(n, \gamma) - (\gamma, n)$  equilibrium. After the exhaustion of neutrons these isotopes decay back to the  $\beta$ -stability valley. In this simplified model the capture cross section magnitude plays no role. However it is known [4–6] that for realistic irradiation scenarios the final elemental abundance is sensitive to the actual  $(n, \gamma)$  cross-sections. This is the case for the hot (classical)  $r$  process, due to the role of late captures during the decay back to stability. It is also the case for a cold  $r$ -process, where the formation path is determined by competition between neutron capture and beta decay.

Lacking experimental information, the cross section for these exotic nuclei is typically obtained from Hauser-Feshbach statistical model calculations [7]. This model is based on a few quantities describing average properties of the nucleus: the nuclear level density (NLD), the photon strength function (PSF) and the neutron transmission coefficient (NTC). The PSF determines  $\Gamma_\gamma$ , NTC determines  $\Gamma_n$  and NLD affects both (see Appendix). The parameters describing the dependence of these quantities on various magnitudes are adjusted to experiment close to  $\beta$  stability. It is thus crucial to find means to verify the predictions of the model far from stability. For example, the use of surrogate reactions with radioactive beams has been suggested as a tool to provide experimental constraints on  $(n, \gamma)$  cross sections [8] for unstable nuclei, but its application is very challenging and restricted to nuclei close to stability. On the other hand the study of  $\gamma$ -ray emission from states above  $S_n$  observed in  $\beta$  decay can give quantitative information on  $\Gamma_\gamma / \Gamma_{tot}$  for unstable nuclei. This information can be used to improve neutron capture cross-section estimates for nuclei far away from  $\beta$  stability.

The emission of  $\gamma$  rays from neutron unbound states populated in  $\beta$  decay has been observed in very few cases studied with high-resolution germanium detectors.

It was first detected in 1972 in the decay of  $^{87}\text{Br}$  [9] which remains one of the best studied cases [10–12]. The other cases are:  $^{137}\text{I}$  [13–15],  $^{93}\text{Rb}$  [16–18],  $^{85}\text{As}$  [14, 19],  $^{141}\text{Cs}$  [20],  $^{95}\text{Rb}$  [21],  $^{94}\text{Rb}$  [17],  $^{77}\text{Cu}$  [22], and  $^{75}\text{Cu}$  [23]. In the decay of  $^{87}\text{Br}$  up to a dozen states emitting single  $\gamma$ -rays have been identified within 250 keV above  $S_n$ , with a total intensity of about 0.5% compared with a neutron emission intensity of 2.6%. The observation of relatively intense  $\gamma$ -rays in this measurement was explained as being due to nuclear structure since some of the levels populated could only decay through the hindered emission of a high orbital angular momentum neutron. On the other hand, it was pointed out [24] that a sizable  $\gamma$ -ray emission from neutron unbound states could be a manifestation of Porter-Thomas (PT) statistical fluctuations in the strength of individual transitions. The extremely asymmetric shape of the PT distribution can lead to very large enhancement of the  $\Gamma_\gamma / \Gamma_{tot}$  ratio with respect to the average. However a general characterization of the phenomenon is still lacking, in particular the relative importance of the different mechanisms governing the competition.

It is difficult to pursue these studies using high-resolution  $\gamma$ -ray spectroscopy. Since the  $\beta$  intensity is distributed over many highly excited states, germanium detectors are prone to miss the  $\gamma$ -ray de-excitation intensity, further fragmented over multiple cascades. This has come to be known as the *Pandemonium* effect [25]. Therefore in order to measure the full  $\gamma$  intensity one must resort to the Total Absorption Gamma-ray Spectroscopy (TAGS) technique aimed at detecting cascades rather than individual  $\gamma$  rays. The power of this method to locate missing  $\beta$  intensity has been demonstrated before [26–28]. However its application in the present case is very challenging, since the expected  $\gamma$  branching is very small. As a matter of fact previous attempts at the Leningrad Nuclear Physics Institute (LNPI) [17] did not lead to clear conclusions. In this work we propose and demonstrate for the first time the use of the TAGS technique to study  $\beta$ -delayed neutron emitters and extract accurate information that can be used to constrain  $(n, \gamma)$  cross-section estimates for very unstable nuclei.

For this study we selected three known neutron emitters:  $^{87}\text{Br}$ ,  $^{88}\text{Br}$  and  $^{94}\text{Rb}$ . The relevant decay parameters are given in Table I. The quoted quantities:  $T_{1/2}$  (half life),  $P_n$  (neutron emission probability),  $Q_\beta$  and  $S_n$  are taken from the ENSDF data base [29–31]. The case of  $^{87}\text{Br}$  has been included in the study on purpose since it allows a comparison of our results with high resolution decay measurements [12] and with neutron capture and transmission experiments [12, 32]. The case of  $^{93}\text{Rb}$  was also measured and will be presented separately [33].

The results of our TAGS analysis are also relevant for reactor decay heat and anti-neutrino spectrum calculations.

The knowledge of the heating produced by radioactive products in a reactor and the time evolution after reactor shutdown is important for reactor safety. In con-

TABLE I. Half-life  $T_{1/2}$ , neutron emission probability  $P_n$ , decay energy window  $Q_\beta$ , and daughter neutron separation energy  $S_n$  for each measured isotope. Values taken from Ref. [29–31].

Isotope	$T_{1/2}$ (s)	$P_n$ (%)	$Q_\beta$ (MeV)	$S_n$ (MeV)
$^{87}\text{Br}$	55.65(13)	2.60(4)	6.852(18)	5.515(1)
$^{88}\text{Br}$	16.34(8)	6.58(18)	8.975(4)	7.054(3)
$^{94}\text{Rb}$	2.702(5)	10.18(24)	10.281(8)	6.828(10)

ventional reactors the decay heat (DH) is dominated by fission products (FP) for cooling times up to a few years. An issue in reactor DH studies has been the persistent failure of summation calculations to reproduce the results of integral experiments for individual fissioning systems. Summation calculations are based on individual FP yields and average  $\gamma$ -ray and  $\beta$  energies retrieved from evaluated nuclear data bases. In spite of this deficiency summation calculations remain an important tool in reactor safety studies. For example, after the Fukushima Dai-ichi nuclear plant accident it was pointed out [34] that summation calculations are relevant to understand the progression of core meltdown in this type of event. The Fukushima accident was the consequence of a failure to dissipate effectively the DH in the reactor core and in the adjacent spent fuel cooling pool. Summation calculations are particularly important in design studies of innovative reactor systems (Gen IV reactors, Accelerator Driven Systems) with unusual fuel compositions (large fraction of minor actinides), high burn ups and/or harder neutron spectra, since integral data are missing.

Yoshida and Nakasima [35] recognized that the *Pandemonium* systematic error is responsible for a substantial fraction of the discrepancy between DH integral experiments and calculations. *Pandemonium* has the effect of decreasing the average  $\gamma$ -ray energy and increasing the average  $\beta$  energy when calculated from available level scheme information obtained in high resolution measurements. The average  $\gamma$  and  $\beta$  energy for each isotope,  $\bar{E}_\gamma$  and  $\bar{E}_\beta$  respectively, can be computed from  $I_\beta(E_x)$ , the  $\beta$  intensity distribution as a function of excitation energy  $E_x$  as

$$\bar{E}_\gamma = \int_0^{Q_\beta} I_\beta(E_x) E_x dE_x \quad (1)$$

$$\bar{E}_\beta = \int_0^{Q_\beta} I_\beta(E_x) \langle E_\beta(Q_\beta - E_x) \rangle dE_x \quad (2)$$

Here  $\langle E_\beta(Q_\beta - E_x) \rangle$  represents the mean value of the  $\beta$  energy continuum leading to a state at  $E_x$ .

The TAGS technique, free from *Pandemonium*, was applied in the 1990s by Greenwood and collaborators at INEL (Idaho) [18] to obtain accurate average decay energies for up to 48 FP with impact in DH calculations.

Recognizing the importance of this approach to improve summation calculations, the OECD/NEA Working Party on International Evaluation Cooperation (WPEC) established subgroup SG25 to review the situation [36]. They made recommendations, in the form of priority lists, for future TAGS measurements on specific isotopes for the U/Pu fuel cycle. The work was later extended to the Th/U fuel cycle by Nichols and collaborators [37]. Subsequently, the results of Algora *et al.* [38] demonstrated the large impact of new TAGS measurements for a few isotopes selected from the priority list.

From the nuclei included in the present work  $^{87}\text{Br}$  was assigned priority 1 in Ref. [36, 37] for a TAGS measurement, although it is an example of a well studied level scheme [29] with up to 374  $\gamma$  transitions de-exciting 181 levels. The justification for the high priority comes from: 1) the large uncertainty (25%) on average energies coming from the spread of intensity normalization values between different measurements, 2) a potential *Pandemonium* error suggested by the number of observed levels at high excitation energies (less than half of the expected number according to level density estimates), and 3) the large contribution to DH around 100 s cooling time.  $^{88}\text{Br}$  also has priority 1 in Ref. [36, 37]. It contributes significantly to the DH at cooling times around 10 s. The known decay scheme [30] is rather incomplete above  $E_x = 3.5$  MeV, from level density considerations, as shown in the RIPL-3 reference input parameter library web page [39]. We estimate that more than 300 levels should be populated in the decay above  $E_x = 3.5$  MeV and below  $S_n$  in comparison with the observed number of 33.  $^{94}\text{Rb}$  is not included in the priority list of Ref. [36] but is considered of relative importance in Refs. [37] and [40] for short cooling times. The decay scheme is very poorly known [31]. Only 37 levels are identified above  $E_x = 3.4$  MeV, regarded as the maximum energy with a complete level scheme [39]. We estimate that more than 900 levels could be populated below  $S_n$  thus pointing to a potentially strong *Pandemonium* effect.

Summation calculations are also a valuable tool to study reactor anti-neutrino  $\bar{\nu}_e$  spectra. Accurate knowledge of this spectrum is of relevance for the analysis of neutrino oscillation experiments [41, 42] and for exploring the use of compact anti-neutrino detectors in nuclear proliferation control [43]. Summation calculations for the  $\bar{\nu}_e$  spectrum suffer from the same problem as DH summation calculations: inaccuracies in fission yields and individual precursor decay data.

For each fission product the electron antineutrino spectrum  $S_{\bar{\nu}}(E_{\bar{\nu}})$ , and the related  $\beta$  spectrum  $S_\beta(E_\beta)$ , can be computed from the  $\beta$  intensity distribution

$$S_{\bar{\nu}}(E_{\bar{\nu}}) = \int_0^{Q_\beta} I_\beta(E_x) s_{\bar{\nu}}(Q_\beta - E_x, E_{\bar{\nu}}) dE_x \quad (3)$$

$$S_\beta(E_\beta) = \int_0^{Q_\beta} I_\beta(E_x) s_\beta(Q_\beta - E_x, E_\beta) dE_x \quad (4)$$

where  $s_{\bar{\nu}}(Q_{\beta} - E_x, E_{\bar{\nu}})$  and  $s_{\beta}(Q_{\beta} - E_x, E_{\beta})$  represent the shape of  $\bar{\nu}_e$  and  $\beta$  energy distributions for the transition to a state at  $E_x$ , which depends on the nuclear wave functions. For each  $E_x$ ,  $s_{\bar{\nu}}$  and  $s_{\beta}$  are related by energy-conservation  $E_{\bar{\nu}} = Q_{\beta} - E_x - E_{\beta}$  to a good approximation [44]. Thus distortions of the observed  $I_{\beta}(E_x)$  distribution in high-resolution  $\gamma$ -ray spectroscopy due to *Pandemonium* tend to produce calculated  $\bar{\nu}_e$  spectra shifted to high energies.

Currently the most reliable reactor  $\bar{\nu}_e$  spectra are obtained from integral  $\beta$ -spectrum measurements of  $^{235}\text{U}$ ,  $^{239}\text{Pu}$  and  $^{241}\text{Pu}$  thermal fission performed by Schreckenbach *et al.* at ILL-Grenoble [45, 46]. Data on  $^{238}\text{U}$  fast fission also became available recently [47]. The conversion of integral  $\beta$  spectra to  $\bar{\nu}_e$  spectra requires a number of approximations. These are needed because, as pointed out above, the transformation is isotope and level dependent. The global conversion procedure has been revised and improved recently [48, 49]. As a consequence of this revision a change of normalization in the spectrum is found that contributes to a consistent deficit when comparing  $\bar{\nu}_e$  rates from short base line experiments with calculations [50], a surprising effect which is termed the reactor neutrino anomaly. The effect has been related to an abundance of transitions of the first forbidden type with a  $\beta$  spectrum departing from the allowed shape [51]. The experimental investigation of this or similar effects requires accurate measurements of individual fission products and the use of the summation method as was argued in [52].

The statistics accumulated in the three running reactor  $\bar{\nu}_e$  experiments, Double Chooz [53], RENO [54] and Daya Bay [55], has revealed differences between the shape of the calculated  $\bar{\nu}_e$  spectra and the measured one. The observed excess between 5 and 7 MeV  $E_{\bar{\nu}_e}$  could be due to the contribution of a few specific FP [56, 57] which is not reproduced by the global conversion method. Thus the study of this new antineutrino shape distortion requires the use of the summation method and reinforces the need for new accurate decay data with the TAGS technique. As a matter of fact one of the key isotopes in this list,  $^{92}\text{Rb}$ , was part of the same experiment analyzed here and its impact on the antineutrino spectrum was already evaluated [58].

Another approach to the improvement of decay data for  $\bar{\nu}_e$  summation calculations was followed in the past by Tengblad *et al.* [59]. They measured the spectrum of electrons emitted in the decay of individual FP using charged particle telescopes. Measurements were performed for up to 111 fission products at ISOLDE (Geneva) and OSIRIS (Studsvik). The  $\beta$  spectra are converted into  $\bar{\nu}_e$  spectra and both are tabulated for 95 isotopes in Ref. [60]. This large set of data is free of *Pandemonium* and can be used both in decay-heat and antineutrino spectrum summation calculations. It was pointed out by O. Bersillon during the work of WPEC-SG25 [36] that average  $\beta$  energies from Tengblad *et al.* [59] can be compared with average  $\beta$  energies calculated from TAGS data obtained

by Greenwood *et al.* [18] for up to 18 fission products. The comparison shows that  $\bar{E}_{\beta}$  energies from Tengblad *et al.* are systematically larger than those from Greenwood *et al.*. The average difference is +177 keV with a spread of values from -33 keV to +640 keV. In view of the relevance of both sets of data it is important to confirm the discrepancy and investigate possible causes. The list of measured isotopes in [59, 60] includes  $^{87,88}\text{Br}$  and  $^{94}\text{Rb}$  thus they can be compared with our data.

Partial results of the work presented here were already published in Ref. [61]. There we concentrated on the  $\beta$ -intensity distribution above  $S_n$  and the possible impact on  $(n, \gamma)$  cross section estimates for unstable neutron-rich nuclei. Here we present these results in greater detail and enhance them with the investigation of new sources of systematic error. In addition we present the complete  $\beta$  intensity distributions and discuss their relevance in relation to reactor decay-heat and anti-neutrino spectrum calculations.

## II. MEASUREMENTS

The measurements were performed at the Cyclotron Laboratory of the University of Jyväskylä. The isotopes of interest are produced by proton-induced fission of Uranium in the ion-guide source of the IGISOL Mass Separator [62]. The mass separated beam is guided to the JYFLTRAP Penning Trap [63], for suppression of contamination. The JYFLTRAP mass resolving power of few tens of thousands is sufficient to select the isotope of interest from the rest of isobars. The beam coming out of the trap is implanted at the centre of the spectrometer onto a movable tape, in between two rollers holding the tape in place. A cross-sectional view of the detection setup is shown in Fig. 1. During the measurements the beam gate is open for a time period equivalent to three half-lives. This optimizes the counting of parent decays over descendant decays. After this period of time the tape transports the remaining activity away and a new measuring cycle starts. The tape moves inside an evacuated aluminium tube of 1 mm thickness and 47 mm diameter. Behind the tape implantation point is placed a 0.5 mm thick Si detector with a diameter of 25 mm, mounted on the aluminium end-cap. The  $\beta$  detection efficiency of the Si detector is about 30%. The Valencia-Surrey Total Absorption Spectrometer “Rocinante” is a cylindrical 12-fold segmented  $\text{BaF}_2$  detector with a length and external diameter of 25 cm, and a longitudinal hole of 5 cm diameter. Each  $\text{BaF}_2$  crystal is optically isolated by means of a thin reflector wrapping, and viewed by a single 3” photo-multiplier tube (PMT). The crystals are mounted inside the aluminium housing which has a 0.8 mm thick wall around the central hole. The total efficiency of “Rocinante” for detecting a single  $\gamma$  ray with the setup described here is larger than 80% in the energy range of interest. The spectrometer is surrounded by 5 cm thick lead shielding to reduce the

detection of the ambient background signals.

The new spectrometer has a reduced neutron sensitivity compared to existing instruments based on NaI(Tl) crystals. This is a key feature in the present measurements as will be shown later. In addition, the segmentation of the detector allows one to obtain information on  $\gamma$ -ray cascade multiplicities which helps in the data analysis. The signal amplitudes from the 12 independent PMTs are digitized in a peak sensing analog-to-digital converter (ADC) and stored on disk for each event. The event trigger is provided whenever the hardware sum of the PMT signals fires a constant fraction discriminator (CFD). The signal from the Si detector is processed in an analogous manner providing another trigger for read-out and storage of events. In the off-line analysis the PMT signals are gain matched and those surpassing a common threshold of 65 keV are added to obtain the total absorption spectrum. The gain-matching procedure uses as a reference the position of the  $\alpha$ -peaks visible in the energy spectra coming from the Ra contamination always present in BaF<sub>2</sub> crystals. In order to eliminate this intrinsic background as well as the ambient background we use in the present analysis  $\beta$ -gated total absorption spectra. The threshold in the Si  $\beta$  detector is set to 100 keV. Nevertheless other sources of background need to be taken into account.

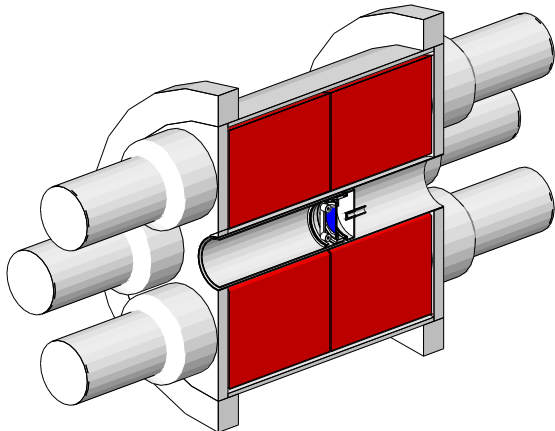


FIG. 1. (Color online) Cross-sectional view of the detector geometry. BaF<sub>2</sub> crystals in red. Si detector in blue. The beam enters from the left and is deposited on the tape (not shown) in front of the Si detector.

Firstly there is the decay descendant contamination, which was computed using Monte Carlo (MC) simulations performed with the Geant4 simulation toolkit [64]. In the case of daughter decay we use an event generator based on  $\beta$  intensity distributions and  $\gamma$  branching ratios obtained from the well known [29–31] decay scheme. The normalization of the daughter contamination is estimated from the known half-lives and the measurement cycle time information and eventually adjusted to provide the best fit to the recorded spectrum. The measurement of <sup>88</sup>Br was accidentally contaminated with <sup>94</sup>Y, the long-

lived grand-daughter of <sup>94</sup>Rb that was measured immediately beforehand. It was treated in the same manner.

The contamination due to the  $\beta$ -delayed neutron branch is more challenging. The decay simulation must explicitly include the neutrons emitted. These neutrons interact with detector materials producing  $\gamma$ -rays through inelastic and capture processes, which are readily detected in the spectrometer. A specific event generator was implemented which reproduces the known neutron energy distribution, taken from [65], and the known  $\gamma$ -ray intensity in the final nucleus, taken from [29–31]. The event generator requires the  $\beta$  intensity distribution followed by neutron emission  $I_{\beta n}(E_x)$  and the branching to each level in the final nucleus. We have used the simplifying assumption that this branching is independent of the excitation energy in the daughter nucleus to obtain  $I_{\beta n}(E_x)$  from the neutron spectrum. The deconvolution of the neutron spectrum using calculated  $\Gamma_\gamma$  and  $\Gamma_n$  within the Hauser-Feshbach model (see below) leads to similar  $I_{\beta n}(E_x)$  but does not reproduce the  $\gamma$  intensity in the final nucleus. Another issue is whether the interaction of neutrons with the detector can be simulated accurately. We have shown recently [66] this to be the case for a LaBr<sub>3</sub>:Ce detector, provided that Geant4 is updated with the newest neutron data libraries and the original capture cascade generator is substituted by an improved one based on the nuclear statistical model. We have followed the same approach for our BaF<sub>2</sub> detector. The normalization factor of the  $\beta$ -delayed neutron decay contamination is fixed by the  $P_n$  value.

Another important source of spectrum distortion is the summing-pileup of events. If more than one event arrives within the same ADC event gate, a signal with the wrong energy will be stored in the spectrum. Apart from the electronic pulse pile-up effect for a single crystal, which can be calculated using the methodology described in [67], one must consider the summing of signals from different crystals. A new Monte Carlo procedure to calculate their combined contribution has been developed. The procedure is based on the superposition of two recorded events, selected randomly. The time of arrival of the second event is sampled randomly within the ADC gate length. The normalization of the resulting summing-pileup spectrum is fixed by the true rate and the ADC gate length [67]. To calculate the rate a dead time correction is necessary and this is obtained by counting the signals from a fixed frequency pulse generator feeding the preamplifier. The use of real events to calculate the spectrum distortion is valid if the actual summing-pileup rate is small enough. For this reason we kept the overall rate during the measurements below 7 kcps. The method is validated with measurements of laboratory sources.

Several sources, <sup>22</sup>Na, <sup>24</sup>Na, <sup>60</sup>Co and <sup>137</sup>Cs, were used to determine both the energy calibration and the resolution versus energy dependency of the spectrometer. The latter is needed to widen the MC simulated response and is parametrized in the form of a Gaussian with  $\sigma_E = \sqrt{aE + bE^2}$ . The highest calibration point

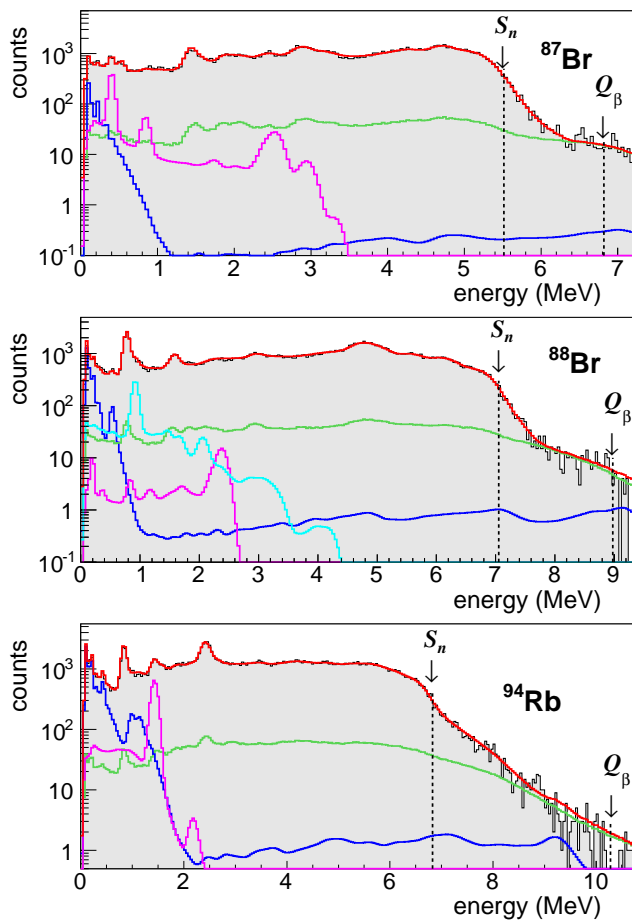


FIG. 2. (Color online) Relevant histograms for the analysis: parent decay (gray filled), daughter decay (pink), delayed neutron decay (dark blue), accidental contamination (light blue), summing-pileup contribution (green), reconstructed spectrum (red). See text for details. The neutron separation energy  $S_n$  and decay energy window  $Q_\beta$  are also indicated.

is at 4.123 MeV. At this energy the energy resolution (FWHM) is 265 keV which becomes 455 keV at 10 MeV. The ungated spectra measured with the sources serve also to verify the accuracy of the Geant4 MC simulations of the spectrometer response to the decay. This requires a detailed description in the simulation code of all materials in the measurement setup (tape transport system and detectors). The use of  $\beta$ -gated spectra in the analysis requires additional verifications of the simulation. Due to the existence of an electronic threshold in the Si detector (100 keV) and the continuum nature of the  $\beta$  spectrum the efficiency for  $\beta$ -detection has a strong dependency with endpoint energy up to about 2 MeV. It should be noted that this affects the spectral region above  $S_n$  in which we are particularly interested. To investigate whether the MC simulation can reproduce this energy dependency accurately we used the information from a separate experiment [68] measuring  $P_n$  values with the neutron counter BELEN and the same  $\beta$

detector and implantation setup. Several  $\beta$ -delayed neutron emitters with known neutron energy spectra were measured, including  $^{88}\text{Br}$ ,  $^{94,95}\text{Rb}$  and  $^{137}\text{I}$ . They have different neutron emission windows  $Q_\beta - S_n$ , therefore the neutron-gated  $\beta$  efficiency samples different portions of the low energy part of the efficiency curve. Indeed the measured average  $\beta$  detection efficiency for each isotope changes by as much as 25%. Using the above mentioned  $\beta$ -delayed neutron decay generator in Geant4 we are able to reproduce the isotope dependent efficiency to within better than 4%, determining the level of accuracy of the simulation.

Figure 2 shows the  $\beta$ -gated TAGS spectrum measured for all three isotopes. Also shown is the contribution to the measured spectra of the daughter decay, the neutron decay branch, and the summing-pileup effect. In the case of  $^{88}\text{Br}$  it also includes the contribution of the accidental contamination with  $^{94}\text{Y}$  decay. Note that there are net counts above the background beyond the neutron separation energy. The fraction of counts that are to be attributed to states above  $S_n$  populated in the decay de-exciting by  $\gamma$ -ray emission is obtained after deconvolution with the spectrometer response. In this region the major background contribution comes from summing-pileup which is well reproduced by the calculation as can be observed. The contribution of neutron capture  $\gamma$ -rays in the detector materials is much smaller, thanks to the low neutron sensitivity of  $\text{BaF}_2$ , as can be seen. The contribution of  $\gamma$ -rays coming from neutron inelastic scattering is important at energies below 1 MeV.

### III. ANALYSIS

The analysis of the  $\beta$ -gated spectra follows the method developed by the Valencia group [69, 70]. The deconvolution of spectra with the spectrometer response to the decay is performed using the Expectation-Maximization (EM) algorithm described there. The spectrometer response is constructed in two steps. First the response to electromagnetic cascades is calculated from a set of branching ratios and the MC calculated response to individual  $\gamma$ -rays. In the simulation we use a single crystal low energy threshold of 65 keV from experiment. When necessary, the electron conversion process is taken into account while building the response [71]. Branching ratios are taken from [29–31] for the low energy part of the level scheme. In the present case this involves 4 levels up to 1.6 MeV for  $^{87}\text{Kr}$ , 8 levels up to 2.5 MeV for  $^{88}\text{Kr}$  and 11 levels up to 2.8 MeV for  $^{94}\text{Sr}$ . The excitation energy range above the last discrete level is treated as a continuum and is divided into 40 keV bins. Average branching ratios for each bin are calculated from the NLD and PSF as prescribed by the nuclear statistical model. We use the NLD calculated using a Hartree-Fock-Bogoliubov (HFB) plus combinatorial approach adjusted to experimental information [39, 72], which includes parity dependence. The PSF is obtained from Generalized Lorentzian

(E1 transitions) or Lorentzian (M1 and E2 transitions) parametrization using the parameters recommended in the RIPL-3 reference input parameter library [39]. In the second step of the response construction, the previously obtained electromagnetic response for each level or energy bin is convoluted with the simulated response to a  $\beta$  continuum of allowed shape. The  $\beta$  response is obtained under the condition that the energy deposited in the Si detector is above the 100 keV threshold.

The spins and parities of some of the discrete states in the daughter nucleus are ambiguous but they are needed in order to calculate the branching ratio from states in the continuum. In the analysis different spin-parity values are tested and those giving the best fit to the spectrum are taken. The spin and parity of the parent nucleus ground state is also uncertain, however it determines the spin and parity of the states populated in the continuum needed to construct the branching ratio matrix. We assume that the Gamow-Teller selection rule applies for decays into the continuum, i.e., the parity does not change and the spin change fulfill  $|\Delta J| \leq 1$ . In the calculation of the branching ratios we further assume that different spins  $J$  are populated according to the spin statistical weight  $2J + 1$ . Our choices of spin and parity for the ground state are  $3/2^-$  for  $^{87}\text{Br}$ ,  $1^-$  for  $^{88}\text{Br}$  and  $3^-$  for  $^{94}\text{Rb}$ , based again on the quality of reproduction of the measured spectra. The spin-parity of  $^{87}\text{Br}$  is given as  $3/2^-$  in Ref. [29], however Ref. [73] proposes  $5/2^-$ . We do not find significant differences in the analysis assuming these two values and we choose the former. The spin-parity of  $^{88}\text{Br}$  is uncertain and is given as  $(2^-)$  in Ref. [30]. However Ref. [74] suggests  $1^-$ . In our analysis we use the latter value since it clearly provides a much better reproduction of the measured TAGS spectrum. In the case of  $^{94}\text{Rb}$   $3(-)$  is proposed [31] and is adopted, since other alternatives did not lead to a better reproduction of the spectrum.

In the analysis we permit decays to all discrete states, many of which are of the forbidden type. Forbidden transitions to the ground state or low lying excited states are known to occur in this region of the nuclear chart. Indeed sizable decay intensity for some forbidden transitions is obtained in our analysis. In the case of  $^{87}\text{Br}$  we find a ground state intensity  $I_{\beta}^{gs} = 10.1\%$  quite close to 12%, the quoted value in Ref. [29]. However in contrast to [29], the first four excited states included in the discrete part receive negligible intensity. The summed decay intensity to the discrete part becomes 51% of that in Ref. [29]. In Ref. [30] an upper limit of 11% is given for the  $^{88}\text{Br}$  ground state decay intensity, and a sizable intensity is quoted for some of the eight excited states included in the analysis. We obtain 4.7% and 5.6% for the  $\beta$  intensity to the ground state and first excited state respectively, and small or negligible intensity for the remaining states. Overall the intensity to this part of the level scheme is reduced by 64%. No intensity is assigned in [31] to  $^{94}\text{Rb}$  decaying to the ground state (third forbidden) and first excited state (first forbidden). In our

analysis we forbid the decay to those states after verifying that the decay intensity obtained when left free is only 0.5% and 0.02% respectively. A large decay intensity of 23.7% is observed for the allowed transition to the state at  $E_x = 2414$  keV, even larger than the value of 21.4% found in [31]. The intensity to the discrete level scheme included in our analysis (11 states) is 78% of that in ENSDF.

In the final analysis we applied a correction to branching ratios deduced from the statistical model. The aim is to obtain a spectrometer response that is as realistic as possible. We scale the calculated branching ratios going from the unknown part of the level scheme to discrete levels in the known part of the level scheme, in order to reproduce the observed  $\gamma$ -ray intensities as tabulated in Ref. [29–31]. Here we are making the assumption that the absolute  $\gamma$  intensity is correctly determined in the high resolution measurements for the lowest excited levels. We found that this adjustment did not lead to significant changes in the quality of reproduction of the measured TAGS spectra and has a small impact on the results of the deconvolution.

Figure 3 shows the final  $\beta$  intensity distribution  $I_{\beta\gamma}(E_x)$  resulting from the deconvolution of TAGS spectra for all three isotopes with the chosen branching ratio matrices. The intensity is normalized to  $(100 - P_n)\%$ . In each case the spectrum reconstructed with this intensity distribution gives a good reproduction of the measured spectrum as can be seen in Fig. 2. The full  $\beta$  intensity distribution including statistical uncertainties is given as Supplemental Material to this article [75]. The uncertainty due to the statistics in the data is computed according to the prescription given in Ref. [70] and is very small.

We evaluate the impact of several sources of systematic uncertainty on the shape of the  $\beta$  intensity distribution. These include both uncertainties in the calculated decay response and uncertainties in the subtraction of background components. To study their effect we follow a similar procedure in all the cases. The chosen systematic parameter is varied and a new deconvolution is performed until we observe an appreciable deterioration in the reproduction of the measured spectrum. This is quantified by the increase of chi-square between the measured and reconstructed spectra. In this way we obtain the maximum acceptable deviation of the  $I_{\beta\gamma}(E_x)$  from the adopted solution for each investigated systematic uncertainty. As a reference the maximum chi-square increase is always below 5%.

Uncertainties in the calculated decay response are of two types. Uncertainties in the branching ratio matrix, which were discussed above, and uncertainties in the MC simulation of the response to  $\gamma$  and  $\beta$  radiation. As already explained we take great care to describe accurately the geometry used in the Geant4 simulation, which is validated from the comparison with measurements with laboratory sources. However these sources emit  $\beta$  particles with rather small energy and they are not useful



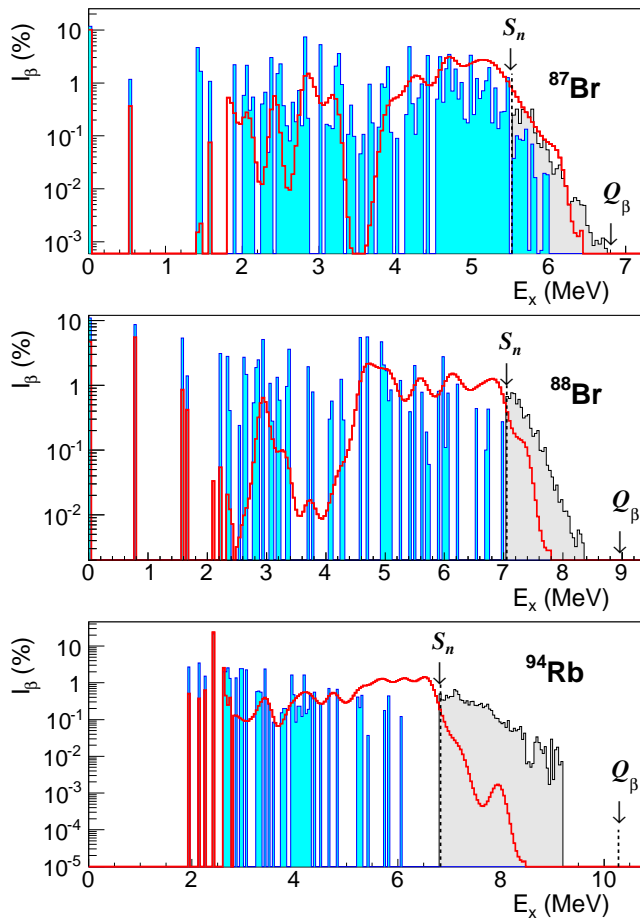


FIG. 3. (Color online) Beta intensity distributions: TAGS result (red line), high-resolution measurements (blue filled), from delayed neutron spectrum (gray filled). See text for details.

to verify the  $\beta$  response. The simulated  $\beta$  efficiency of the Si detector and in particular its variation with end-point energy was studied in a separate measurement [68] as already discussed. The response of the spectrometer to  $\beta$  particles depositing energy in the Si is not easy to verify. The response is a mixture of  $\beta$  penetration and secondary radiation produced in dead materials. The accurate simulation of the interaction of low energy electrons is a challenging task for any MC code. They rely on models to describe the slowing down of electrons and changes in their trajectory. Typically a number of tracking parameters are tuned to obtain reliable results. We use in the present simulations the *Livermore Electromagnetic Physics List* of Geant4 (version 9.2.p2) with original tracking parameters. This physics list has been developed for high accuracy tracking of low energy particles. We verified that limiting the tracking step length (parameter *StepMax*) to values much smaller than default values, increased computing time considerably but did not significantly affect the simulated response. To study the effect of a possible systematic error on the  $\beta$  response

we take a pragmatic approach. We scale arbitrarily the simulated spectrometer response while keeping the same  $\beta$  efficiency. In this way we find that solutions corresponding to changes of  $\pm 10\%$  in the  $\beta$  response normalization represent the maximum deviation with respect to the adopted solution that can be accepted.

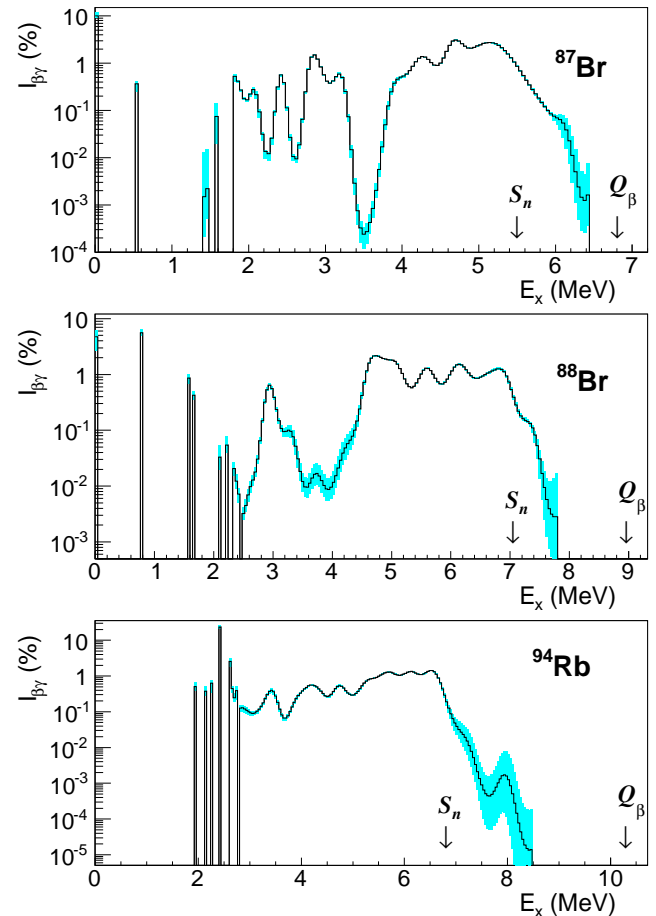


FIG. 4. (Color online) Beta intensity distributions from TAGS. The thin black line is the adopted solution, the light blue filled region indicates the spread of solutions due to the systematic effects investigated. See text for details.

The individual  $\gamma$  response is well tested up to  $E_\gamma = 2.754$  MeV, the maximum energy for the  $^{24}\text{Na}$  source. To investigate the effect of a possible systematic error in the total  $\gamma$  efficiency  $\varepsilon_\gamma$  or in the peak-to-total ratio (P/T) we introduce a model that varies linearly one of the two parameters,  $\varepsilon_\gamma$  or P/T, above  $E_\gamma = 3$  MeV. We found that variations of  $\varepsilon_\gamma$  amounting to  $\pm 15\%$  at  $E_\gamma = 10$  MeV or variations of P/T amounting to  $\pm 30\%$  at the same energy are the maximum allowed by good reproduction of the spectrum. When considering these numbers one should bear in mind that the de-excitation of highly excited states populated in the decay of the three isotopes proceeds with an average  $\gamma$  multiplicity of 2 to 4 in such a way that the energy of most  $\gamma$  rays in the decay does not exceed 3 MeV.



Uncertainties in the normalization of background components also have an impact on the  $\beta$  intensity distribution. We consider the two main components, summing-pileup which affects the high energy part of the spectrum, and the  $\beta$ -delayed neutron decay branch, which affects the low energy part of the spectrum (see Fig. 2). The component due to summing-pileup is normalized using the same ADC gate length ( $5 \mu\text{s}$ ) for all three isotopes. We estimate however that the reproduction of the end-part of the spectra allows for a variation of up to  $\pm 15\%$  in the normalization factor. The normalization of the  $\beta$ -delayed neutron decay component is fixed by the  $P_n$  value. Likewise we find that the reproduction of the low energy part of the spectrum allows for a variation of up to  $\pm 15\%$  in the normalization factor.

Finally we also check the impact on the result associated with the use of a different deconvolution algorithm, by using the Maximum Entropy Method as described in Ref. [70]. This leads to changes in the  $I_\beta(E_x)$  noticeable both at the high-energy end and at low  $E_x$ .

There is no straightforward way to quantify and combine the systematic uncertainties associated with the effects investigated. One of the reasons is that they are not independent since we are requiring reproduction of the data. It would have been a formidable task to explore in a correlated way the full parameter space. We use a different point of view here. The solutions we obtain through the systematic variation of each parameter represent maximum deviations from the adopted solution, thus altogether define an estimate of the space of solutions compatible with the data. This is represented in a graphical way in Fig. 4 showing the envelope of the different solutions described above corresponding to the maximum accepted deviation from the adopted solution. In total there are 14 solutions for  $^{87}\text{Br}$ , 13 for  $^{88}\text{Br}$ , and 15 for  $^{94}\text{Rb}$ . As can be seen the different solutions differ little except for specific  $E_x$  regions, where the  $\beta$  intensity is low, in particular at the high energy end of the distribution or at low excitation energy.

#### IV. AVERAGE BETA AND GAMMA DECAY ENERGIES AND DECAY HEAT

Figure 3 shows in addition to  $I_{\beta\gamma}(E_x)$  obtained from our TAGS data the intensity obtained from high-resolution measurements retrieved from the ENSDF data base [29–31]. The effect of *Pandemonium* is visible here. Our results show a redistribution of  $I_{\beta\gamma}(E_x)$  towards high  $E_x$ , which is significant for  $^{87}\text{Br}$ , and very large for  $^{88}\text{Br}$  and  $^{94}\text{Rb}$ . This is even clearer in the accumulated  $\beta$  intensity distribution as a function of excitation energy  $I_{\beta\gamma}^\Sigma(E_x) = \int_0^{E_x} I_{\beta\gamma}(E) dE$ , depicted in Fig. 5. The intensity is normalized to  $100\% - P_n$  except in the case of the  $^{94}\text{Rb}$  ENSDF intensity that only reaches 59.8% since the evaluators of Ref. [31] recognize the incompleteness of the decay scheme.

Table II shows  $\bar{E}_\gamma$  and  $\bar{E}_\beta$  obtained from  $I_{\beta\gamma}(E_x)$  us-

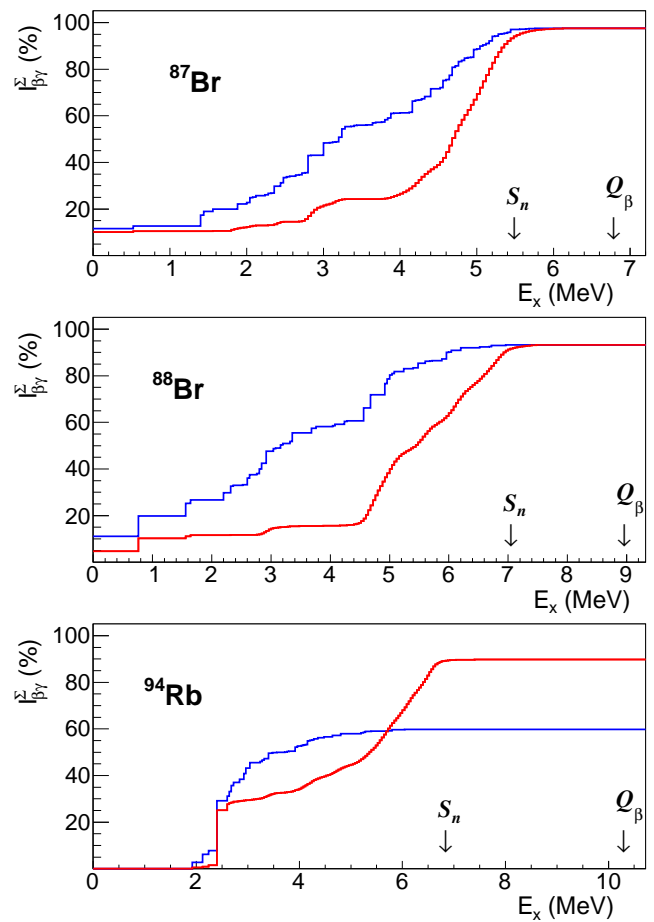


FIG. 5. (Color online) Accumulated  $\beta$  intensity distribution  $I_{\beta\gamma}^\Sigma$ : TAGS result (red line), high-resolution measurements (blue line).

ing Eq. 1 and Eq. 2 respectively. The  $\beta$  continuum and its average energy  $\langle E_\beta(Q_\beta - E_x) \rangle$  for each  $E_x$  is calculated using subroutines extracted from the LOGFT program package maintained by NNDC (Brookhaven) [76]. In the calculations we assume an allowed  $\beta$  shape. As can be seen in Table II the redistribution of  $\beta$  intensity leads to large differences in the average emission energies when comparing high resolution data (ENSDF) and the present TAGS data. The difference has opposite directions for  $\gamma$  and  $\beta$  energies, as expected, except in the case of  $^{94}\text{Rb}$  due to the use of a different normalization. For  $\bar{E}_\gamma$  the difference is 0.9 MeV for  $^{87}\text{Br}$ , 1.7 MeV for  $^{88}\text{Br}$ , and 2.3 MeV for  $^{94}\text{Rb}$ . The uncertainty quoted on the TAGS average energies in Table II is systematic since the contribution of statistical uncertainties in the case of  $I_{\beta\gamma}(E_x)$  is negligible. The values of  $\bar{E}_\gamma$  and  $\bar{E}_\beta$  were computed for each intensity distribution that was used to define the space of accepted solutions in Fig. 4, and the maximum positive and negative difference with respect to the adopted solution is the value quoted in the Table.

TABLE II. Average  $\gamma$  and  $\beta$  energies calculated using  $I_{\beta\gamma}(E_x)$  intensity distributions from ENSDF [29–31] and present TAGS data. The contribution of the  $\beta$ -delayed neutron branch is not included.

Isotope	$\bar{E}_\gamma$ (keV)		$\bar{E}_\beta$ (keV)	
	ENSDF	TAGS	ENSDF	TAGS
$^{87}\text{Br}$	3009	$3938^{+40}_{-67}$	1599	$1159^{+32}_{-19}$
$^{88}\text{Br}$	2892	$4609^{+78}_{-67}$	2491	$1665^{+32}_{-38}$
$^{94}\text{Rb}$	1729	$4063^{+62}_{-66}$	2019	$2329^{+32}_{-30}$

Table III shows the  $\bar{E}_\beta$  given in Ref. [60] obtained from the  $\beta$  spectrum measurements of Tengblad *et al.* [59]. For comparison the average  $\beta$  energy obtained from the present TAGS data, given in Table II, is incremented with the average  $\beta$  energy corresponding to the  $\beta$  delayed neutron branch. The contribution of the  $\beta n$  branch is calculated from the  $I_{\beta n}(E_x)$  distribution obtained as explained in Section II. We find that the values of [60] agree with our result for  $^{88}\text{Br}$  but differ by 240 keV for  $^{87}\text{Br}$  and by 380 keV for  $^{94}\text{Rb}$ . This situation is comparable to that observed for Greenwood *et al.* [18] TAGS data. Figure 6 presents in a graphical way the difference of average  $\beta$  energies  $\Delta\bar{E}_\beta$  between the results of Tengblad *et al.* and the results of both Greenwood *et al.* and ourselves. In the figure the differences are represented as a function of  $Q_\beta$  to illustrate what seems a systematic trend. Although the scattering of values is relatively large, on average the differences are smaller below  $\sim 5$  MeV. The isotopes from Ref. [18] shown in Fig. 6 are:  $^{146}\text{Ce}$ ,  $^{145}\text{Ce}$ ,  $^{144}\text{Ba}$ ,  $^{141}\text{Ba}$ ,  $^{143}\text{La}$ ,  $^{94}\text{Sr}$ ,  $^{93}\text{Sr}$ ,  $^{145}\text{La}$ ,  $^{143}\text{Ba}$ ,  $^{89}\text{Rb}$ ,  $^{141}\text{Cs}$ ,  $^{145}\text{Ba}$ ,  $^{91}\text{Rb}$ ,  $^{95}\text{Sr}$ ,  $^{140}\text{Cs}$ ,  $^{90}\text{Rb}$ ,  $^{90m}\text{Rb}$ , and  $^{93}\text{Rb}$ , in order of increasing  $Q_\beta$ .

TABLE III. Comparison of average  $\beta$  energies obtained from direct  $\beta$  spectrum measurement (Tengblad *et al.* [60]) with those obtained combining  $I_{\beta\gamma}(E_x)$  from present TAGS data and  $I_{\beta n}(E_x)$  derived from neutron spectrum data. See text for details.

Isotope	$\bar{E}_\beta$ (keV)	
	This work	Ref. [60]
$^{87}\text{Br}$	$1170^{+32}_{-19}$	$1410 \pm 10$
$^{88}\text{Br}$	$1706^{+32}_{-38}$	$1680 \pm 10$
$^{94}\text{Rb}$	$2450^{+32}_{-30}$	$2830 \pm 70$

More illustrative than the comparison of average values is the comparison of  $\beta$  energy distributions  $S_\beta(E_\beta)$  as is done in Fig. 7. Large differences in shape between the results of Tengblad *et al.* and the present TAGS results are clearly seen, even for  $^{88}\text{Br}$  where the average values agree. The contribution of the  $\beta$ -delayed neutron branch, added to the TAGS result for the comparison, is shown. For reference we also include in the fig-

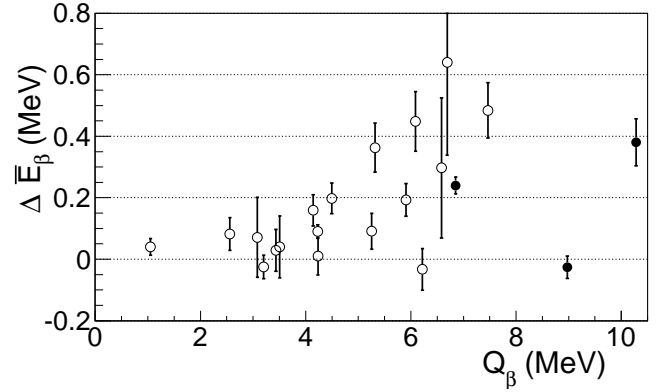


FIG. 6. Difference between average  $\beta$  energies obtained by direct  $\beta$  spectrum measurements (Tengblad *et al.* [60]) and from TAGS  $\beta$  intensity distributions. TAGS results are from [18] (open circles) and from the present work (filled circles).

ure the distribution calculated from the high-resolution level scheme in ENSDF. The  $S_\beta(E_\beta)$  distribution calculated from the TAGS data is shifted to lower energies for the three isotopes, in comparison to the direct  $\beta$  spectrum measurement. We should point out that a similar trend is found for the remaining isotopes included in the same experimental campaign,  $^{86}\text{Br}$  and  $^{91}\text{Rb}$  [77], and  $^{92,93}\text{Rb}$  [33, 58], where we find deviations in  $\Delta\bar{E}_\beta$  in the range 200 to 400 keV. Moreover, our results for  $^{91}\text{Rb}$  and  $^{93}\text{Rb}$  agree rather well with those obtained by Greenwood *et al.* [18].

The assumption of an allowed shape used here to calculate  $S_\beta(E_\beta)$  from  $I_\beta(E_x)$  introduces some uncertainty in the comparison. However it is likely to be a good approximation. Thus to explain the difference between TAGS results and the direct  $\beta$  spectrum measurement one is forced to consider systematic errors in the use of either one of the two techniques or both. As explained above we investigated carefully sources of systematic uncertainty which can lead to distortions of the  $\beta$  energy distribution and found that none of them can explain the observed differences (see Table III). Moreover as shown in Fig. 4 the measured TAGS spectrum imposes a strong constraint on the bulk of the  $\beta$  intensity distribution. It is difficult to imagine additional sources of systematic uncertainty which can have a significant impact on the shape of this distribution. To clarify the discrepancy new measurements of the spectrum of  $\beta$  particles emitted in the decay of a number of selected isotopes would be of great value.

To finalize this part of the discussion we should point out that  $\bar{E}_\gamma$  can be obtained from the  $\beta$  spectra measured in [59]. This can be achieved by deconvolution of the  $\beta$  spectra with appropriate  $\beta$  shapes  $s_\beta(Q_\beta - E_x, E)$  to obtain the  $I_\beta(E_x)$  (see Eq. 4). As a matter of fact this procedure is needed (and applied in [59]) to obtain the antineutrino spectrum using Eq. 3. The average  $\gamma$  energies obtained in this way would show systematic dif-

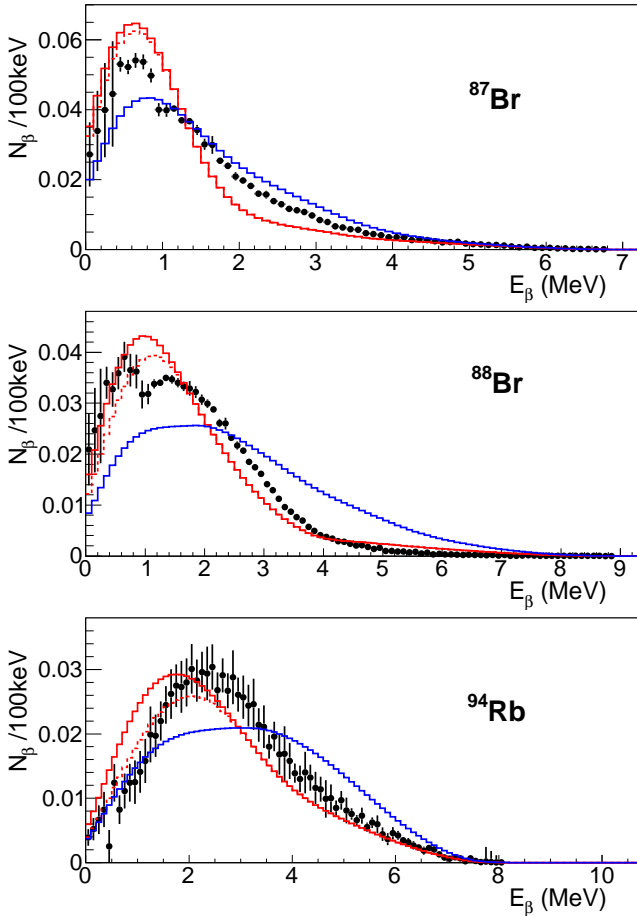


FIG. 7. (Color online) Comparison of  $\beta$  spectra  $S_\beta$ . Tengblad *et al.* [60]: black circles; present TAGS result: dashed red line; present TAGS plus  $\beta$  delayed neutron contribution: continuous red line; high-resolution measurements [29–31]: blue line.

ferences with respect to TAGS results of opposite sign to those found for  $\bar{E}_\beta$ . Rather than using this approach the authors of [60] determine average  $\gamma$  energies  $\bar{E}_\gamma$  from an independent set of measurements using a NaI(Tl) detector to obtain the spectrum of  $\gamma$ -rays for the decay of each isotope. There are also large discrepancies between these results and those obtained from TAGS measurements. We postpone the discussion of these differences to a forthcoming publication [77].

The impact of the present TAGS results for  $\bar{E}_\gamma$  and  $\bar{E}_\beta$  on decay-heat summation calculations was evaluated. Figure 8 shows the ratio of calculations using TAGS data to calculations using high-resolution data. The figure shows the evolution of the ratio as a function of cooling time following the prompt thermal fission of  $^{235}\text{U}$  and  $^{239}\text{Pu}$ . Both together account for most of the power released in most reactors. The calculation is similar to that described in Ref. [57]. It uses fission yields from JEFF-3.1 [78] and the ENDF/B-VII updated decay data sublibrary. The update introduces  $\beta$ -intensity distribu-

tions from previous TAGS measurements and, for a few isotopes, from  $\beta$ -spectrum measurements and from theoretical calculations. As is customary the DH is evaluated separately for the electromagnetic energy (EEM), or photon component ( $\gamma$  rays, X rays, ...), and for the light particle energy (ELP), or electron component ( $\beta$  particles, conversion electrons, Auger electrons, ...). The ratio is computed for each individual isotope and for the three isotopes together. As expected the effect of the inclusion of TAGS data is largest for  $^{94}\text{Rb}$  and smallest for  $^{87}\text{Br}$ . The largest variation in the EEM component occurs at short cooling times between 1 and 10 s. Due to the particular normalization of the high-resolution  $^{94}\text{Rb}$   $\beta$ -intensity distribution mentioned above the effect is not observed in the ELP component (see also Table II). The effect is larger for  $^{235}\text{U}$  fission, due to the larger fission yields for the three isotopes, reaching an increment of 3.3% for the combined contribution to the EEM component at  $t = 3.5$  s. For  $^{239}\text{Pu}$  the increment reaches 1.8%. Although the impact is somewhat small the present data contribute to reduce the discrepancy between DH integral measurements and summation calculations for  $^{235}\text{U}$  in the range of 1 to 100 s (see for example Fig. 12 of Ref. [79]).

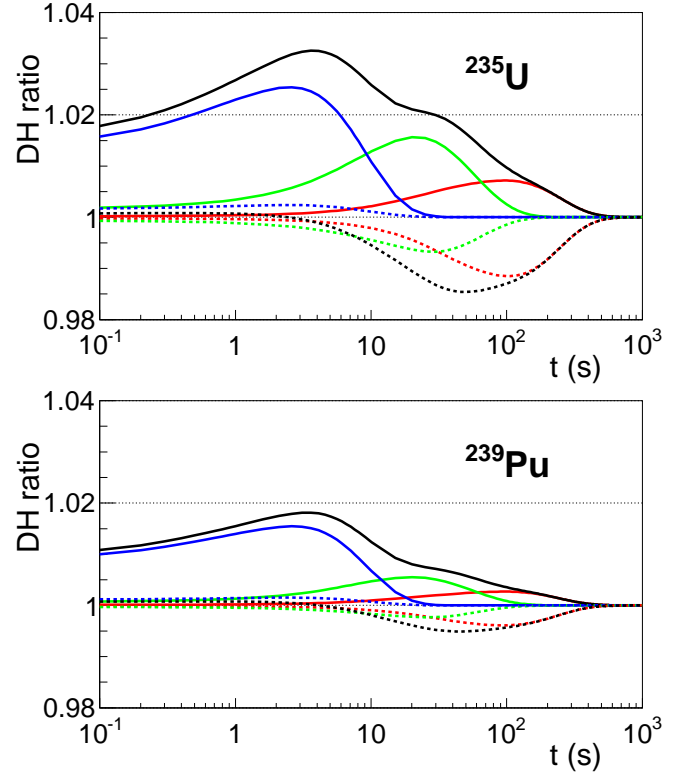


FIG. 8. (Color online) Ratio of decay heat as a function of cooling time calculated for  $^{235}\text{U}$  and  $^{239}\text{Pu}$  when our TAGS data replaces high-resolution data. Continuous line: photon component; dashed line: electron component. Red:  $^{87}\text{Br}$ ; green:  $^{88}\text{Br}$ ; blue:  $^{94}\text{Rb}$ ; black: all three isotopes.

## V. ANTINEUTRINO SPECTRA

The impact of our data on calculated antineutrino spectrum is shown in Fig. 9 and Fig. 10. The  $\bar{\nu}_e$  summation calculation of Fig. 9 is analogous to the DH calculation of Fig. 8. It shows for  $^{235}\text{U}$  and  $^{239}\text{Pu}$  fission the ratio of calculated  $\bar{\nu}_e$  spectrum when our TAGS data replaces the high resolution data. The effect of each individual isotope and of the three together is shown. For both fissioning systems the impact of  $^{87}\text{Br}$  is negligible, while the effect of  $^{88}\text{Br}$  peaks around 8.5 MeV (3%) and that of  $^{94}\text{Rb}$  peaks around 7 MeV (4%). The combined effect is a reduction of the calculated  $\bar{\nu}_e$  spectrum which reaches a value of 6% around 7.2 MeV. Similar figures are obtained for  $^{238}\text{U}$  and  $^{241}\text{Pu}$ . It is remarkable that the effect of our TAGS data for  $^{88}\text{Br}$  and  $^{94}\text{Rb}$  is of equal importance to that of the combined effect of recently measured [80] TAGS data for  $^{92}\text{Rb}$ ,  $^{96}\text{Y}$  and  $^{142}\text{Cs}$ . Compare Fig. 9 in the present work with Fig. 6 of Ref. [80], which shows an effect of similar shape and magnitude. These three isotopes contribute most to the  $\bar{\nu}_e$  spectrum around 7 MeV, with  $^{92}\text{Rb}$  being the largest contributor [58]. Due to current uncertainties in the summation method it is not easy to draw conclusions on the impact of both experiments on the origin of the antineutrino spectrum shape distortion. Note that they lead to a *reduction* of the calculated spectrum which is maximum about 1 MeV above the center of the observed *excess*. Better quality data for a larger set of isotopes, including decay data and fission yields, is required. Our result shows the importance of performing TAGS measurements for fission products with very large  $Q_\beta$ -value, which are likely to be affected by large *Pandemonium* systematic error, even if they have moderate fission yields.

Figure 10 shows a different set of  $\bar{\nu}_e$  summation calculations. The calculation is analogous to that described in Ref. [52]. It uses a different selection of decay data from the calculation shown in Fig. 9. More specifically it uses antineutrino spectra derived from the  $\beta$  spectra of Tengblad *et al.* [59] for  $^{87,88}\text{Br}$  and  $^{94}\text{Rb}$  instead of  $\bar{\nu}_e$  spectra derived from high-resolution data. Thus Fig. 10 shows the effect of replacing Tengblad *et al.* data with our TAGS data. As can be seen the replacement of  $^{87}\text{Br}$  has little impact, while there is a cancellation below  $E_{\bar{\nu}_e} = 8$  MeV between the  $^{88}\text{Br}$  and  $^{94}\text{Rb}$  deviations. However the difference between our TAGS data and the data of Tengblad *et al.* for  $^{88}\text{Br}$  produces an increase in the calculated antineutrino spectra of about 7% between 8 and 9 MeV. Note that although  $^{94}\text{Rb}$  has a  $Q_\beta$  of 10.28 MeV we do not observe appreciable  $\beta$  intensity below 2.41 MeV excitation energy, thus the maximum effective endpoint energy is below 8 MeV. The relatively large impact of  $^{88}\text{Br}$  is due to the fact that only a few decay branches contribute to the spectrum here. Note that in this energy interval the uncertainty of the integral  $\beta$ -spectrum measurements [45, 46] is relatively large, thus summation calculations are particularly relevant. This points again to the need to perform TAGS measurements

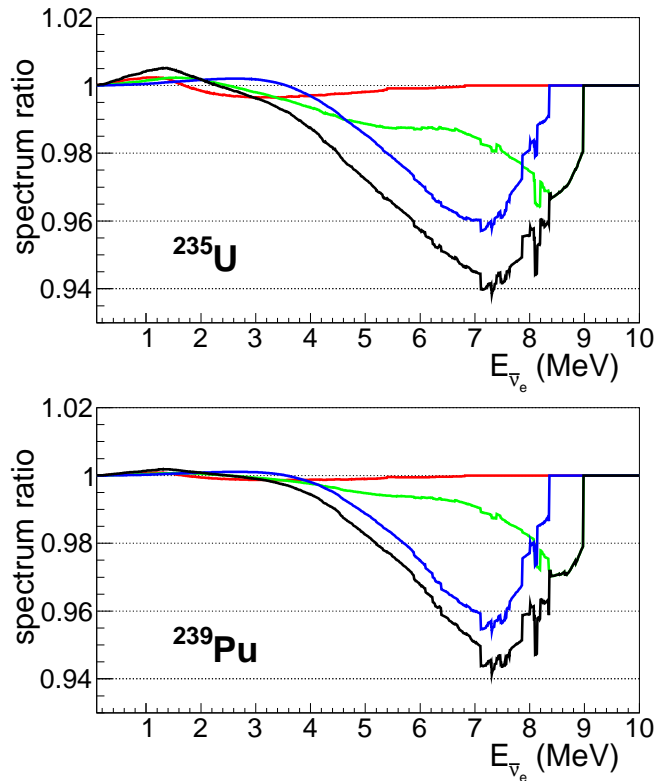


FIG. 9. (Color online) Ratio of antineutrino spectra as a function of energy calculated for  $^{235}\text{U}$  and  $^{239}\text{Pu}$  when our TAGS data replaces high-resolution data. Red:  $^{87}\text{Br}$ ; green:  $^{88}\text{Br}$ ; blue:  $^{94}\text{Rb}$ ; black: all three isotopes.

for fission products with very large  $Q_\beta$ .

## VI. GAMMA INTENSITY FROM NEUTRON UNBOUND STATES

Figure 3 shows for all three isotopes a sizable TAGS intensity  $I_{\beta\gamma}(E_x)$  above  $S_n$ . This intensity extends well beyond the first few hundred keV where the low neutron penetrability makes  $\gamma$ -ray emission competitive. For comparison the figure includes the  $\beta$ -intensity distribution followed by neutron emission  $I_{\beta n}(E_x)$  deduced from the neutron spectrum as explained above. The integrated decay intensity above  $S_n$  followed by  $\gamma$ -ray emission  $P_\gamma = \int_{S_n}^{Q_\beta} I_{\beta\gamma}(E_x) dE_x$  obtained from the TAGS measurement is compared to the integrated  $I_{\beta n}(E_x)$  or  $P_n$  value in Table IV. Surprisingly large values of  $P_\gamma$  are obtained, which in the case of  $^{87}\text{Br}$  is even larger than  $P_n$ . The  $\gamma$  branching represents 57% of the total for  $^{87}\text{Br}$ , 20% for  $^{87}\text{Br}$  and 4.5% for  $^{94}\text{Rb}$ . In the case of  $^{87}\text{Br}$  we find 8 times more intensity than the high-resolution experiment [12], which can be explained by the *Pandemonium* effect. The quoted uncertainty on the TAGS integrated intensity  $P_\gamma$  is completely dominated by systematic uncertainties since the uncertainty due to data statistics is

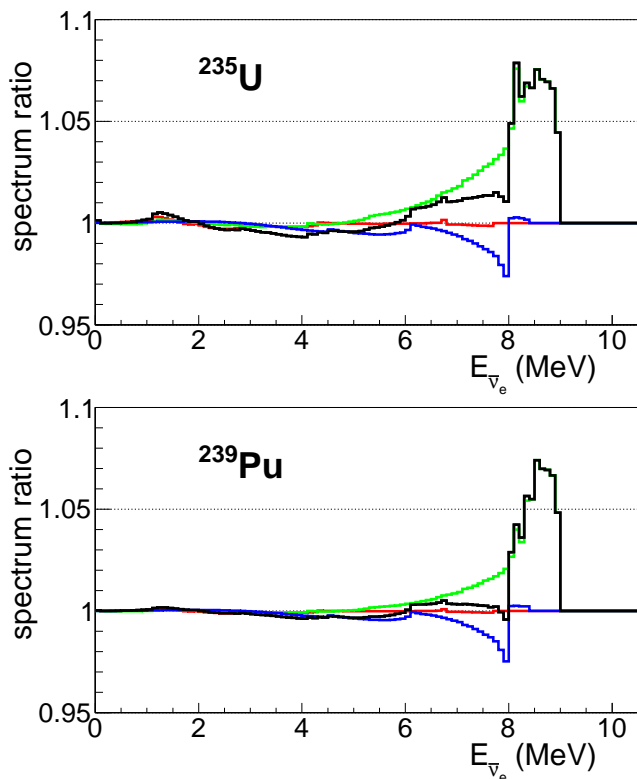


FIG. 10. (Color online) Ratio of antineutrino spectra as a function of energy calculated for  $^{235}\text{U}$  and  $^{239}\text{Pu}$  when our TAGS data replaces the data Tengblad *et al.* Red:  $^{87}\text{Br}$ ; green:  $^{88}\text{Br}$ ; blue:  $^{94}\text{Rb}$ ; black: all three isotopes.

below 0.6% (relative value) in all cases.

TABLE IV. Integrated  $\beta$ -intensity  $P_\gamma$  from TAGS data above  $S_n$  compared to  $P_n$  values from [29–31].

Isotope	$P_\gamma$ (%)	$P_n$ (%)
$^{87}\text{Br}$	$3.50^{+49}_{-40}$	2.60(4)
$^{88}\text{Br}$	$1.59^{+27}_{-22}$	6.4(6)
$^{94}\text{Rb}$	$0.53^{+33}_{-22}$	10.18(24)

We have evaluated several sources of systematic uncertainty. In the first place we consider uncertainties that affect the overall  $\beta$  intensity distributions, which were already detailed in Section III. To quantify the uncertainties in  $P_\gamma$  coming from the spread of possible solutions compatible with the data (see Fig 4) we follow the approach used in Section IV and take the maximum positive and negative difference with respect to the adopted solution as a measure of this uncertainty.

In addition to this we consider other sources of uncertainty which mostly affect the integral value.

A possible source of uncertainty is related to the correlations introduced by the finite energy resolution in the

deconvolution process. This can cause a relocation of counts in a region of rapidly changing intensity [70], such as the region around  $S_n$ . However we estimate from a model deconvolution that this effect is not relevant in the present case. Likewise the uncertainty on width calibration also has an impact on the redistribution of counts around  $S_n$ . The highest width calibration point is at 4.123 MeV. From the comparison of different fits, varying the number and distribution of calibration points, we determine that the extrapolation of the calibration curve can vary by up to  $\pm 15\%$  at 10 MeV. This introduces an uncertainty in  $P_\gamma$  of 2% for  $^{87}\text{Br}$  and 6% for  $^{88}\text{Br}$  and  $^{94}\text{Rb}$ .

The uncertainty in the energy calibration of TAGS spectra might have an impact on the result because of the dependence of the response on energy. However we verified that this effect is negligible. The main effect of the uncertainty on the energy calibration is on the integration range. Since the intensity is rapidly changing in the region around  $S_n$  the effect can be large. The fact that the structure observed in the distribution of Fig. 11 around 7–8 MeV for  $^{94}\text{Rb}$  coincides with the levels populated in the final nucleus (see next Section) allows us to conclude that the energy calibration at  $S_n$  is correct to about one energy bin (40 keV). We evaluate the uncertainty in the integral, equivalent to changes of half a bin, to be 11% for the bromine isotopes and 15% for rubidium.

The uncertainty values entered in Table IV correspond to the sum in quadrature of the three types of uncertainty mentioned above: uncertainties in the deconvolution, and uncertainties in the resolution and energy calibration.

## VII. COMPARISON WITH HAUSER-FESHBACH CALCULATIONS

We show in Fig. 11 the ratio  $I_{\beta\gamma}(E_x)/(I_{\beta\gamma}(E_x) + I_{\beta n}(E_x))$  as a function of excitation energy. The shaded area represents the uncertainty in the ratio coming from the spread of solutions  $I_{\beta\gamma}(E_x)$  to the TAGS inverse problem shown in Fig. 4. It should be noted that the ratio is affected also by systematic uncertainties in the  $I_{\beta n}(E_x)$  distribution coming from the deconvolution of neutron experimental spectra as well as by uncertainties in the neutron spectra themselves, but they are not considered here.

The experimental intensity ratio in Fig. 11 is identical to the average ratio  $\langle \Gamma_\gamma(E_x)/\Gamma_{\text{tot}}(E_x) \rangle$ . The average is taken over all levels in each bin populated in the decay. Thus the experimental distribution can be directly compared with the results of Hauser-Feshbach calculations of this ratio. The NLD and PSF used in the calculations are the same as used to construct the spectrometer response to the decay (see Section III). The new ingredient needed is the NTC which is obtained from the Optical Model (OM). It is calculated with Raynal’s ECIS06 OM code integrated in the TALYS-1.4 software pack-



age [81]. OM parameters are taken from the so-called local parametrization of Ref. [82]. Neutron transmission is calculated for final levels known to be populated in the decay: g.s. of  $^{86}\text{Kr}$ , g.s and first excited state of  $^{87}\text{Kr}$ , and g.s. plus 8 excited states of  $^{93}\text{Sr}$ . With these ingredients one obtains the average widths  $\langle\Gamma_\gamma\rangle$  and  $\langle\Gamma_n\rangle$  (see Appendix).

In the case of  $^{87}\text{Kr}$  we can compare the calculated average values with experimental data obtained from neutron capture and transmission reactions [12, 32]. In particular for  $1/2^-$  and  $3/2^-$  resonances which are populated in the decay of a  $3/2^-$   $^{87}\text{Br}$  ground state. Up to fifty  $1/2^-$  and sixty-six  $3/2^-$  resonances were identified in an interval of 960 keV above  $S_n$ . The NLD of Ref. [72] predicts 46 and 90 respectively, in fair agreement with these values. The distribution of neutron widths for  $1/2^-$  resonances in the interval  $E_n = 250 - 960$  keV is compatible with a PT distribution with average width  $\langle\Gamma_n\rangle = 1.95$  keV. The same is true for  $3/2^-$  resonances with  $\langle\Gamma_n\rangle = 2.79$  keV. In the same interval the Hauser-Feshbach calculated widths vary between 0.3 keV and 0.7 keV for  $1/2^-$  states and between 0.5 keV and 0.9 keV for  $3/2^-$  states. In both cases the calculation is about 4 times too low. The information on  $\langle\Gamma_\gamma\rangle$  is less abundant. The  $\gamma$  width has been determined for six  $1/2^-$  and ten  $3/2^-$  resonances, with values in the range 0.075-0.48 eV, and is fixed to 0.255 eV, from systematics, for the remaining resonances. The Hauser-Feshbach calculation gives values in the range 0.08-0.12 eV. On average the calculation is about a factor three too low. Since the NLD reproduces the number of resonances, to reach such values for the partial widths requires a renormalization by a factor of 3-4 for the PSF and the NTC in  $^{87}\text{Kr}$ , which seems large. The reader should note that variations of similar magnitude and direction for both the PSF and NTC have little impact on the calculated ratio  $\langle\Gamma_\gamma/\Gamma_{tot}\rangle$ . It should also be noted that this ratio is insensitive to changes in NLD.

We show in Fig. 11 the ratio  $\langle\Gamma_\gamma/\Gamma_{tot}\rangle$ , calculated with nuclear statistical parameters as described above, for the three spin-parity groups populated under the Gamow-Teller selection rule. Due to statistical fluctuations affecting individual widths [24], this cannot be obtained as  $\langle\Gamma_\gamma\rangle/(\langle\Gamma_\gamma\rangle + \langle\Gamma_n\rangle)$ . Rather than trying to obtain a formula for the average correction factor to be applied to this ratio, which is the common practice for cross section calculations [81], we use the Monte Carlo method to obtain directly the average of width ratios. The procedure to obtain a statistical realization (or sample) from the model is similar to that described in Ref. [69]. Level energies for each spin-parity are generated according to a Wigner distribution from the NLD. For each state the corresponding  $\Gamma_\gamma$  and  $\Gamma_n$  to individual final states are sampled from PT distributions with the calculated average values (see Appendix). The total  $\gamma$  and neutron widths are obtained by summation over all possible final states and the ratio is computed. The ratio is averaged for all levels lying within each energy bin (40 keV).

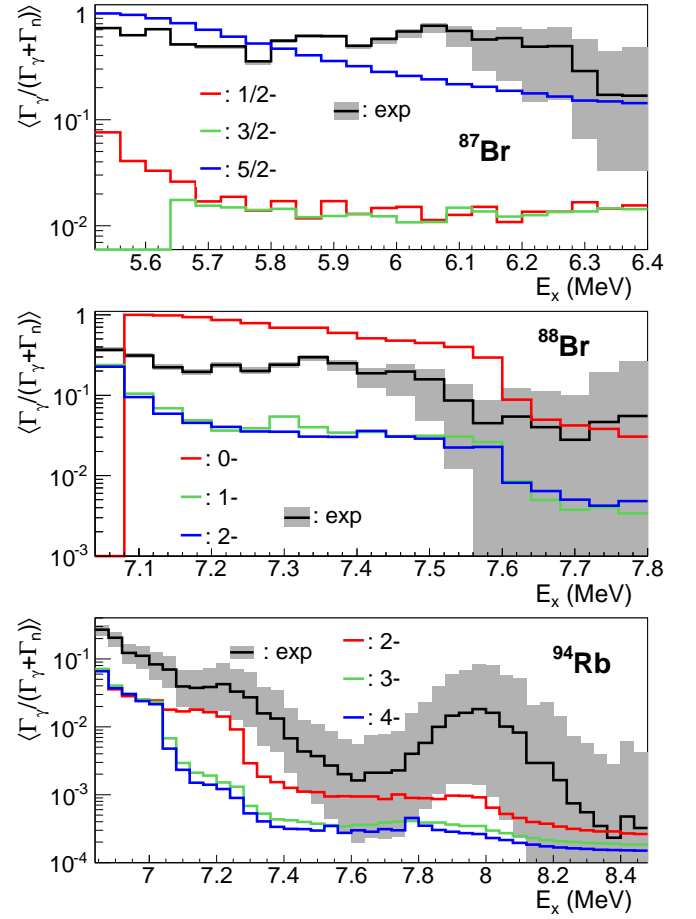


FIG. 11. (Color online) Average gamma to total width from experiment (black line) and calculated for the three spin-parity groups populated in allowed decay (red, green, blue). The gray-shaded area around the experiment indicates the sensitivity to systematic effects. See text for details.

In order to eliminate fluctuations in the calculated averages, the procedure is repeated between 5 and 1000 times depending on level density. Very large average enhancement factors are obtained, reaching two orders-of-magnitude, when the neutron emission is dominated by the transition to a single final state.

In the case of the decay of the  $3/2^-$  ground state in  $^{87}\text{Br}$  one can see in Fig. 11 that the strong  $\gamma$ -ray emission above  $S_n$  can be explained as a consequence of the large hindrance of  $l = 3$  neutron emission from  $5/2^-$  states in  $^{87}\text{Kr}$  to the  $0^+$  g.s. of  $^{86}\text{Kr}$ . This is the explanation already proposed in [12]. The situation is even more favorable to this explanation if the spin-parity of  $^{87}\text{Br}$  were  $5/2^-$  as suggested in [73]. In this case the neutron emission is hindered for both  $5/2^-$  and  $7/2^-$  states populated in the allowed decay. In the case of  $^{88}\text{Br}$   $1^-$  decay a similar situation occurs for  $0^-$  states in  $^{88}\text{Kr}$  below the first excited state in  $^{87}\text{Kr}$  at 532 keV, which requires  $l = 3$  neutron emission to populate the  $5/2^+$  g.s. in  $^{87}\text{Kr}$ . It should be noted that if the spin-parity of  $^{88}\text{Br}$

were  $2^-$  as suggested in [30] the three allowed spin-parity groups ( $1^-$ ,  $2^-$ ,  $3^-$ ) will have similar gamma-to-total ratios, a factor of 3 to 5 too low compared to experiment, which reinforces our choice of  $1^-$  for the  $^{88}\text{Br}$  g.s. A more quantitative comparison of the experimental and calculated ratios requires a knowledge of the distribution of  $\beta$  intensity between the three spin groups. This can be obtained from  $\beta$  strength theoretical calculations, such as those in [83] for example. It is clear however that for both bromine isotopes the large  $\gamma$  branching above  $S_n$  can be explained as a nuclear structure effect: the absence of states in the final nucleus which can be populated through the emission of neutrons of low orbital angular momentum.

The case of  $^{94}\text{Rb}$   $3^-$  decay is the most interesting. The final nucleus  $^{93}\text{Sr}$  is five neutrons away from  $\beta$  stability. Although the  $\gamma$  intensity is strongly reduced, only 5 % of the neutron intensity, is detectable up to more than 1 MeV above  $S_n$ . The structure observed in the distribution of the average ratio  $\langle \Gamma_\gamma / \Gamma_{tot} \rangle$ , can be associated with the opening of  $\beta n$  channels to different excited states in  $^{93}\text{Sr}$ . As can be seen the structure is reproduced by the calculation, which confirms the energy calibration at high excitation energies. In any case the calculated average gamma-to-total ratio is well below the experimental value. In order to bring the calculation in line with the experimental value one would need to enhance the  $\gamma$  width, or suppress the neutron width, or any suitable combination of the two, by a very large factor of about one order-of-magnitude. A large enhancement of the  $\gamma$  width, and thus of the calculated  $(n, \gamma)$  cross sections, would have an impact on  $r$  process abundance calculations [4–6]. It would be necessary to confirm the large enhancement of the  $\langle \Gamma_\gamma / \Gamma_{tot} \rangle$  ratio observed in  $^{94}\text{Rb}$  with similar studies on other neutron-rich nuclei in this mass region as well as in other mass regions. It will also be important to quantify the contribution of a possible suppression of the neutron width to the observed ratio.

## VIII. SUMMARY AND CONCLUSION

We apply the TAGS technique to study the decay of three  $\beta$ -delayed neutron emitters. For this we use a new segmented  $\text{BaF}_2$  spectrometer with reduced neutron sensitivity, which proved to be well suited to this purpose. The three isotopes,  $^{87}\text{Br}$ ,  $^{88}\text{Br}$  and  $^{94}\text{Rb}$ , are fission products with impact in reactor decay heat and antineutrino spectrum summation calculations. We obtain  $\beta$  intensity distributions which are free from the *Pandemonium* systematic error, affecting the data available in the ENSDF data base for the three isotopes. The average  $\gamma$ -ray energies that we obtain are 31%, 59% and 235% larger than those calculated with this data base for  $^{87}\text{Br}$ ,  $^{88}\text{Br}$  and  $^{94}\text{Rb}$  respectively, while the average  $\beta$  energies are 28%, 33% and 13% smaller.

We compare the energy distribution of  $\beta$  particles emitted in the decay derived from our  $\beta$  intensity distribu-

tions with the direct  $\beta$  spectrum measurement performed by Tengblad *et al.*, and find significant discrepancies. Our distributions are shifted to somewhat lower energies. This is reflected in the average  $\beta$  energies, which we find to be 17% and 13% smaller for  $^{87}\text{Br}$  and  $^{94}\text{Rb}$  respectively. Similar systematic differences are found when the TAGS data of Greenwood *et al.* for 18 isotopes is compared with the data of Tengblad *et al.*. We performed a thorough investigation of possible systematic errors in the TAGS technique and find that none of them can explain the observed differences. It will be important to perform new direct measurements of the  $\beta$  spectrum for a few selected isotopes in order to investigate this issue further.

We estimate the effect of the present data on DH summation calculations. We find a relatively modest impact when the high resolution decay data are replaced by our TAGS data. The impact in the photon component is largest at short cooling times. For  $^{235}\text{U}$  thermal fission it reaches an increment of 3.3% around 3.5 s after fission termination. This is mainly due to the decay of  $^{94}\text{Rb}$ . The influence of  $^{88}\text{Br}$  is smaller and peaks at around 25 s. In spite of being small it contributes to reduce the discrepancy between DH integral measurements of the EEM component and summation calculations for  $^{235}\text{U}$  in the range of 1 to 100 s. Many FP contribute in this time range, thus additional TAGS measurements of short lived FP are required to remove the discrepancy. In the case of  $^{239}\text{Pu}$  the maximum increment is about 1.8%.

We also evaluate the impact of the new TAGS data on antineutrino spectrum summation calculations. When our data replace the data from high-resolution measurements we observe a reduction of the calculated  $\bar{\nu}_e$  spectrum which reaches a maximum value of 6% at 7 MeV for the thermal fission  $^{235}\text{U}$ . A similar value is obtained for  $^{239}\text{Pu}$ . The reduction is mainly due to the decay of  $^{94}\text{Rb}$ . The effect of  $^{88}\text{Br}$ , somewhat smaller, peaks at 8.5 MeV. It is remarkable that we find an impact similar to that observed for  $^{92}\text{Rb}$ ,  $^{96}\text{Y}$  and  $^{142}\text{Cs}$  which make the largest contribution to the antineutrino spectrum at these energies. The reason is that the large value of the *Pandemonium* systematic error prevails over the relatively small fission yield for the isotopes studied in this work. We also verified the effect of replacing our TAGS data with Tengblad *et al.*  $\beta$ -spectrum data. We found a relatively small impact below  $E_{\bar{\nu}_e} = 8$  MeV in part due to a compensation effect of the deviations for  $^{94}\text{Rb}$  and  $^{88}\text{Br}$ . However between 8 and 9 MeV the use of TAGS data for  $^{88}\text{Br}$  leads to an increase of about 7% in the calculated antineutrino spectrum. This relatively large impact is due to the small number of decay branches in this energy range. All this underlines the need for TAGS measurements for fission products with a very large  $Q_\beta$  decay energy window.

We confirm the suitability of the TAGS technique for obtaining accurate information on  $\gamma$ -ray emission from neutron-unbound states. In order to assess the reliability of the result we examined the systematic errors



carefully since they dominate the total uncertainty budget. Surprisingly large  $\gamma$ -ray branchings of 57% and 20% were observed for  $^{87}\text{Br}$  and  $^{88}\text{Br}$  respectively. In the case of  $^{94}\text{Rb}$  the measured branching of 4.5% is smaller but still significant. For  $^{87}\text{Br}$  we observe 8 times more intensity than previously detected with high resolution  $\gamma$ -ray spectroscopy, which confirms the need to use the TAGS technique for such studies.

Combining the information obtained from TAGS measurements about the  $\gamma$  intensity from states above  $S_n$  with the  $\beta$ -delayed neutron intensity we can determine the branching ratio  $\langle \Gamma_\gamma / (\Gamma_\gamma + \Gamma_n) \rangle$  as a function of  $E_x$ . The information thus acquired, can be used to constrain the neutron capture cross-section for unstable neutron-rich nuclei. This opens a new field for applications of  $\beta$ -decay TAGS studies. It also provides additional arguments for the need for accurate measurements of  $\beta$ -delayed neutron emission in exotic nuclei. The measurements should cover neutron spectra and yields as well as neutron- $\gamma$  coincidences.

From the comparison of our experimental results with Hauser-Feshbach calculations we conclude that the large  $\gamma$  branching observed in  $^{87}\text{Br}$  and  $^{88}\text{Br}$  is a consequence of the nuclear structure. Some of the resonances populated in the decay can only disintegrate via the emission of a kinematically hindered neutron to the levels available in the final nucleus. A similar situation can occur for other  $\beta$ -delayed neutron emitters, when the number of levels in the final nucleus within the emission window  $Q_\beta - S_n$  is small. It should be noted that such strong  $\gamma$  to neutron competition introduces a large correction to the estimation of  $\beta$ -delayed neutron emission probabilities from  $\beta$ -strength calculations and should be taken into account when comparing experiment with calculation.

The case of  $^{94}\text{Rb}$ , is more representative of the situation expected for nuclei far from stability, where many levels are available thus the decay by low  $l$  neutron emission is always possible. For  $^{94}\text{Rb}$  we find that the  $\gamma$ -ray emission from neutron-unbound states is largely suppressed, but still much larger (an order-of-magnitude) than the result of Hauser-Feshbach calculations using standard parameters for level density, photon strength and neutron transmission. If such enhancement with respect to the Hauser-Feshbach model is due mainly to an increment in the radiative width, then a similar increase is obtained for the neutron capture cross-section. This can have a significant impact on calculated elemental abundances in the astrophysical  $r$  process. It is necessary to confirm and generalize the result obtained for the neutron-rich nucleus  $^{94}\text{Rb}$  extending this type of study to other  $\beta$ -delayed neutron emitters in the same and different mass regions, in particular farther away from the valley of  $\beta$ -stability. Such measurements using the TAGS technique are already underway and additional studies are planned.

## ACKNOWLEDGMENTS

This work was supported by Spanish Ministerio de Economía y Competitividad under grants FPA2008-06419, FPA2010-17142, FPA2011-24553, FPA2014-52823-C2-1-P, CPAN CSD-2007-00042 (Ingenio2010) and the program Severo Ochoa (SEV-2014-0398). WG would like to thank the University of Valencia for support. This work was supported by the Academy of Finland under the Finnish Centre of Excellence Programme 2012-2017 (Project No. 213503, Nuclear and Accelerator-Based Physics Research at JYFL). Work supported by EPSRC(UK) and STFC(UK). Work partially supported by the European Commission under the FP7/EURATOM contract 605203. We thank D. Lhuillier for making available in digital form data tabulated in Ref. [60].

## APPENDIX

The average  $\gamma$  width for initial levels (resonances) of spin-parity  $J_i^\pi$  at excitation energy  $E_x$  can be obtained by summation over all final states of spin-parity  $J_f^\pi$  and excitation energy  $E_x - E_\gamma$ :

$$\langle \Gamma_\gamma(J_i^\pi, E_x) \rangle = \frac{1}{\rho(J_i^\pi, E_x)} \sum_f \sum_{XL} E_\gamma^{2L+1} f_{XL}(E_\gamma) \quad (5)$$

where  $\rho(J_i^\pi, E_x)$  represents the density of initial levels and  $f_{XL}(E_\gamma)$  is the photon strength for transition energy  $E_\gamma$ . The appropriate electric or magnetic character  $X$  and multipolarity  $L$  of the transition is selected by spin and parity conservation. We have used the common practice of restricting the transition types to E1, M1 and E2 with no mixing, which leads to a single  $XL$  choice for each final state.

For transitions into a bin of width  $\Delta E$  in the continuum part of the level scheme the density weighted average over final levels should be used:

$$\langle \Gamma_\gamma(J_i^\pi, E_x) \rangle = \frac{1}{\rho(J_i^\pi, E_x)} \sum_f \sum_{XL} \int_E^{E+\Delta E} E_\gamma^{2L+1} \times f_{XL}(E_\gamma) \rho(J_f^\pi, E_x - E_\gamma) dE_\gamma \quad (6)$$

Likewise the average neutron width can be obtained by summation over all final states of spin-parity  $J_f^\pi$  and excitation energy  $E_x - S_n - E_n$  in the final nucleus:

$$\langle \Gamma_n(J_i^\pi, E_x) \rangle = \frac{1}{2\pi\rho(J_i^\pi, E_x)} \sum_f \sum_{ls} T^{ls}(E_n) \quad (7)$$

where  $T^{ls}(E_n)$  is the neutron transmission coefficient, a function of neutron energy  $E_n$ . The orbital angular momentum  $l$  and channel spin  $s$  are selected by spin and parity conservation for each final level.

- 
- [1] K.L. Kratz *et al.*, *Astron. Astrophys.* **125**, 381 (1983).
- [2] S. Mughabghab, *Atlas of Neutron Resonances* (Elsevier Science, 2006).
- [3] E.M. Burbidge *et al.*, *Rev. Mod. Phys.* **29**, 547 (1957).
- [4] S. Goriely, *Phys. Lett. B* **436**, 10 (1998).
- [5] R. Surman *et al.*, *Phys. Rev. C* **64**, 035801 (2001).
- [6] A. Arcones *et al.*, *Phys. Rev. C* **83**, 045809 (2011).
- [7] T. Rauscher *et al.*, *Atom. Data and Nucl. Data Tables* **75**, 1 (2000).
- [8] J. E. Escher *et al.*, *Rev. Mod. Phys.* **84**, 353 (2012).
- [9] D.R. Slaughter *et al.*, *Phys. Lett. B* **38**, 22 (1972).
- [10] H. Tovedal *et al.*, *Nucl. Phys. A* **252**, 253 (1975).
- [11] F.M. Nuh *et al.*, *Nucl. Phys. A* **293**, 410 (1977).
- [12] S. Raman *et al.*, *Phys. Rev. C* **28**, 602 (1983).
- [13] F.M. Nuh *et al.*, *Phys. Lett. B* **53**, 435 (1975).
- [14] K.L. Kratz *et al.*, *Nucl. Phys. A* **317**, 335 (1979).
- [15] H. Ohm *et al.*, *Z. Phys. A* **296**, 23 (1980).
- [16] C.J. Bischof *et al.*, *Phys. Rev. C* **15**, 1047 (1977).
- [17] G. D. Alkharov *et al.*, Leningrad Nuclear Physics Institute, Preprint 1497 (1989).
- [18] R.C. Greenwood *et al.*, *Nucl. Instrum. Methods Phys. Res., Sect. A* **390**, 95 (1997).
- [19] J.P. Omtvedt *et al.*, *Z. Phys. A* **339**, 349 (1991).
- [20] H. Yamamoto *et al.*, *Phys. Rev. C* **26**, 125 (1982).
- [21] K.L. Kratz *et al.*, *Z. Phys. A* **312**, 43 (1983).
- [22] S.V. Ilyushkin *et al.*, *Phys. Rev. C* **80**, 054304 (2009).
- [23] S.V. Ilyushkin *et al.*, *Phys. Rev. C* **83**, 014322 (2011).
- [24] B. Jonson *et al.*, *Proc. 3rd Int. Conf. on Nuclei far from stability*, CERN Report 76-13 (1976) 277.
- [25] J. Hardy *et al.*, *Phys. Lett. B* **71**, 307 (1977).
- [26] A. Algora *et al.*, *Nucl. Phys. A* **654**, 727c (1999).
- [27] A. Algora *et al.*, *Phys. Rev. C* **68**, 034301 (2003).
- [28] Z. Hu *et al.*, *Phys. Rev. C* **60**, 024315 (1999).
- [29] R. G. Helmer, *Nucl. Data Sheets* **95**, 543 (2002).
- [30] E.A. McCutchan and A.A. Sonzogni, *Nucl. Data Sheets* **115**, 135 (2014).
- [31] D. Abriola and A.A. Sonzogni, *Nucl. Data Sheets* **107**, 2423 (2006).
- [32] R. F. Carlton *et al.*, *Phys. Rev. C* **38**, 1605 (1988).
- [33] A.-A. Zakari-Issoufou, PhD. Thesis, University of Nantes, to be published.
- [34] K. Okumura *et al.*, *Proceedings of the 2012 Symposium on Nuclear Data, Kyoto*, JAEA-Conf 2013-002, INDC(JPN)-198, p. 15, 2013.
- [35] T. Yoshida and R. Nakasima, *J. Nucl. Sci. Technol.*, **18**, 393 (1981).
- [36] T. Yoshida *et al.*, *Assessment of Fission Product Decay Data for Decay Heat Calculations*, OECD/NEA Working Party for International Evaluation Co-operation, Volume 25, 2007.
- [37] M. Gupta *et al.*, *Decay Heat Calculations: Assessment of Fission Product Decay Data Requirements for Th/U Fuel*, IAEA report INDC(NDS)-0577, 2010.
- [38] A. Algora *et al.*, *Phys. Rev. Lett.* **105**, 202501 (2010).
- [39] RIPL-3, R. Capote *et al.*, *Nucl. Data Sheets* **110**, 3107 (2009).
- [40] M. Fleming and J. C. Sublet, *Decay Data Comparisons for Decay Heat and Inventory Simulations of Fission Events*, UK Atomic Energy Authority, Culham Science Centre, CCFE-R(15)28/S1, 2015.
- [41] C. Bemporad *et al.*, *Rev. Mod. Phys.* **74**, 297 (2002).
- [42] S.-B. Kim *et al.*, *Adv. High Energy Phys.* **2013**, 453816 (2013).
- [43] M. Cribier, *Nucl. Phys. B (Proc. Suppl.)* **221**, 57 (2011).
- [44] X. Mougeot, *Phys. Rev. C* **91**, 055504 (2015).
- [45] K. Schreckenbach *et al.*, *Phys. Lett. B* **160**, 325 (1985).
- [46] A. A. Hahn *et al.*, *Phys. Lett. B* **218**, 365 (1989).
- [47] N. Haag *et al.*, *Phys. Rev. Lett.* **112**, 122501 (2014).
- [48] Th. A. Mueller *et al.*, *Phys. Rev. C* **83**, 054615 (2011).
- [49] P. Huber, *Phys. Rev. C* **84**, 024617 (2011).
- [50] G. Mention *et al.*, *Phys. Rev. D* **83**, 073006 (2011).
- [51] D. L. Fang and B.A. Brown, *Phys. Rev. C* **91**, 025503 (2015).
- [52] M. Fallot *et al.*, *Phys. Rev. Lett.* **109**, 202504 (2012).
- [53] Y. Abe *et al.*, *J. High Ener. Phys.* **10**, 086 (2014).
- [54] J. H. Choi *et al.*, *Phys. Rev. Lett.* **116**, 211801 (2016).
- [55] F. P. An *et al.*, *Phys. Rev. Lett.* **116**, 061801 (2016).
- [56] D. A. Dwyer and T. J. Langford, *Phys. Rev. Lett.* **114**, 012502 (2015).
- [57] A. A. Sonzogni *et al.*, *Phys. Rev. C* **91**, 011301 (2015).
- [58] A. A. Zakari-Issoufou *et al.*, *Phys. Rev. Lett.* **115**, 102503 (2015).
- [59] O. Tengblad *et al.*, *Nucl. Phys. A* **503**, 136 (1989).
- [60] G. Rudstam *et al.*, *Atomic Data and Nuclear Data Tables* **45**, 239 (1989).
- [61] J. L. Tain *et al.*, *Phys. Rev. Lett.* **115**, 062502 (2015).
- [62] I. Moore *et al.*, *Nucl. Instrum. Methods Phys. Res., Sect. B* **317**, 208 (2013).
- [63] T. Eronen *et al.*, *Eur. Phys. J. A* **48**, 46 (2012).
- [64] S. Agostinelli *et al.*, *Nucl. Instrum. Methods Phys. Res., Sect. A* **506**, 250 (2003).
- [65] ENDF/B-VII.1, M.B. Chadwick *et al.*, *Nucl. Data Sheets* **112**, 2887 (2011).
- [66] J. L. Tain *et al.*, *Nucl. Instrum. Methods Phys. Res., Sect. A* **774**, 17 (2015).
- [67] D. Cano-Ott *et al.*, *Nucl. Instrum. Methods Phys. Res., Sect. A* **430**, 488 (1999).
- [68] J. Agramunt *et al.*, *Nucl. Instrum. Methods Phys. Res., Sect. A* **807**, 69 (2016).
- [69] J. L. Tain *et al.*, *Nucl. Instrum. Methods Phys. Res., Sect. A* **571**, 719 (2007).
- [70] J. L. Tain *et al.*, *Nucl. Instrum. Methods Phys. Res., Sect. A* **571**, 728 (2007).
- [71] D. Cano-Ott *et al.*, *Nucl. Instrum. Methods Phys. Res., Sect. A* **430**, 333 (1999).
- [72] S. Goriely *et al.*, *Phys. Rev. C* **78**, 064307 (2008).
- [73] M.-G. Porquet *et al.*, *Eur. Phys. J. A* **28**, 153 (2006).
- [74] J. Genevey *et al.*, *Phys. Rev. C* **59**, 82 (1999).
- [75] See Supplemental Material at [link](#) for tables of the  $\beta$  intensity distribution from this work.
- [76] ENSDF Analysis Programs - LOGFT, National Nuclear Data Center, Brookhaven National Laboratory, [http://www.nndc.bnl.gov/nndcscr/ensdf\\_pgm/analysis/logft/](http://www.nndc.bnl.gov/nndcscr/ensdf_pgm/analysis/logft/)
- [77] S. J. Rice, *Decay Heat Measurements of Fission Fragments  $^{86}\text{Br}$ ,  $^{91}\text{Rb}$  and  $^{94}\text{Sr}$  Using Total Absorption Gamma-ray Spectroscopy*, PhD Thesis, University of Surrey, 2014 (to be published).
- [78] A. J. Koning *et al.*, *Journal of the Korean Physical Society* **59**, 1057 (2011).
- [79] D. Jordan *et al.*, *Phys. Rev. C* **87**, 044318 (2013).
- [80] B. C. Rasco *et al.*, *Phys. Rev. Lett.* **117**, 092501 (2016).
- [81] A. J. Koning *et al.*, *Proceedings International Conference*

on Nuclear Data for Science and Technology, April 22-27, 2007, Nice, France, EDP Sciences (2008) 211.

[82] A. J. Koning *et al.*, Nucl. Phys. A **713** (2003) 231

[83] P. Möller *et al.*, Phys. Rev. C **67**, 055802 (2003).